

*Persistent global greening over the last four decades using novel long-term vegetation index data with enhanced temporal consistency.*

Article

Published Version

Creative Commons: Attribution 4.0 (CC-BY)

Open Access

Jeong, S., Ryu, Y., Gentine, P., Lian, X., Fang, J., Li, X., Dechant, B., Kong, J., Choi, W., Jaing, C., Keenan, T. F., Harrison, S. P. ORCID: <https://orcid.org/0000-0001-5687-1903> and Prentice, I. C. (2024) Persistent global greening over the last four decades using novel long-term vegetation index data with enhanced temporal consistency. *Remote Sensing of Environment*, 311. 114282. ISSN 1879-0704 doi: 10.1016/j.rse.2024.114282 Available at <https://centaur.reading.ac.uk/117405/>

It is advisable to refer to the publisher's version if you intend to cite from the work. See [Guidance on citing](#).

To link to this article DOI: <http://dx.doi.org/10.1016/j.rse.2024.114282>

Publisher: Elsevier

All outputs in CentAUR are protected by Intellectual Property Rights law, including copyright law. Copyright and IPR is retained by the creators or other

copyright holders. Terms and conditions for use of this material are defined in the [End User Agreement](#).

[www.reading.ac.uk/centaur](http://www.reading.ac.uk/centaur)

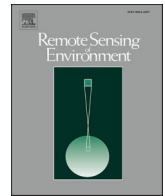
## **CentAUR**

Central Archive at the University of Reading

Reading's research outputs online

Contents lists available at [ScienceDirect](https://www.sciencedirect.com)

## Remote Sensing of Environment

journal homepage: [www.elsevier.com/locate/rse](http://www.elsevier.com/locate/rse)

## Persistent global greening over the last four decades using novel long-term vegetation index data with enhanced temporal consistency

Sungchan Jeong<sup>a,b</sup>, Youngryel Ryu<sup>a,b,c,f,\*</sup>, Pierre Gentine<sup>d,e</sup>, Xu Lian<sup>d</sup>, Jianing Fang<sup>d</sup>,  
Xing Li<sup>f</sup>, Benjamin Dechant<sup>g,h</sup>, Juwon Kong<sup>f,i</sup>, Wonseok Choi<sup>a,b</sup>, Chongya Jiang<sup>j,k</sup>,  
Trevor F. Keenan<sup>l,m</sup>, Sandy P. Harrison<sup>n,p</sup>, Iain Colin Prentice<sup>o,p</sup>

<sup>a</sup> Interdisciplinary Program in Landscape Architecture, Seoul National University, Seoul, Republic of Korea

<sup>b</sup> Integrated Major in Smart City Global Convergence, Seoul National University, Seoul, Republic of Korea

<sup>c</sup> Department of Landscape Architecture and Rural Systems Engineering, Seoul National University, Seoul, Republic of Korea

<sup>d</sup> Department of Earth and Environmental Engineering, Columbia University, New York, NY, USA

<sup>e</sup> Center for Learning the Earth with Artificial intelligence and Physics (LEAP), Columbia University, New York, NY, USA

<sup>f</sup> Research Institute of Agriculture and Life Sciences, Seoul National University, Seoul, Republic of Korea

<sup>g</sup> German Centre for Integrative Biodiversity Research (iDiv), Halle-Jena-Leipzig, Leipzig, Germany

<sup>h</sup> Leipzig University, Leipzig, Germany

<sup>i</sup> Yale School of the Environment, Yale University, New Haven, CT 06511, USA

<sup>j</sup> Agroecosystem Sustainability Center, Institute for Sustainability, Energy, and Environment, University of Illinois at Urbana Champaign, Urbana, IL, USA

<sup>k</sup> Department of Natural Resources and Environmental Sciences, College of Agricultural, Consumer and Environmental Sciences, University of Illinois at Urbana Champaign, Urbana, IL, USA

<sup>l</sup> Climate and Ecosystem Sciences Division, Lawrence Berkeley National Laboratory, Berkeley, CA, USA

<sup>m</sup> Department of Environmental Science, Policy and Management, UC Berkeley, Berkeley, CA, USA

<sup>n</sup> Geography and Environmental Science, University of Reading, Whiteknights, Reading RG6 6AH, United Kingdom

<sup>o</sup> Georgina Mace Centre for the Living Planet, Department of Life Sciences, Imperial College London, Silwood Park Campus, Buckhurst Road, Ascot SL5 7PY, United Kingdom

<sup>p</sup> Ministry of Education Key Laboratory for Earth System Modelling, Department of Earth System Science, Tsinghua University, Beijing 100084, China

## ARTICLE INFO

Editor: Jing M. Chen

## Keywords:

AVHRR  
MODIS  
NDVI  
NIRv  
Greening trend  
Orbital drift

## ABSTRACT

Advanced Very High-Resolution Radiometer (AVHRR) satellite observations have provided the longest global daily records from 1980s, but the remaining temporal inconsistency in vegetation index datasets has hindered reliable assessment of vegetation greenness trends. To tackle this, we generated novel global long-term Normalized Difference Vegetation Index (NDVI) and Near-Infrared Reflectance of vegetation (NIRv) datasets derived from AVHRR and Moderate Resolution Imaging Spectroradiometer (MODIS). We addressed residual temporal inconsistency through three-step post processing including cross-sensor calibration among AVHRR sensors, orbital drifting correction for AVHRR sensors, and machine learning-based harmonization between AVHRR and MODIS. After applying each processing step, we confirmed the enhanced temporal consistency in terms of detrended anomaly, trend and interannual variability of NDVI and NIRv at calibration sites. Our refined NDVI and NIRv datasets showed a persistent global greening trend over the last four decades (NDVI:  $0.0008 \text{ yr}^{-1}$ ; NIRv:  $0.0003 \text{ yr}^{-1}$ ), contrasting with those without the three processing steps that showed rapid greening trends before 2000 (NDVI:  $0.0017 \text{ yr}^{-1}$ ; NIRv:  $0.0008 \text{ yr}^{-1}$ ) and weakened greening trends after 2000 (NDVI:  $0.0004 \text{ yr}^{-1}$ ; NIRv:  $0.0001 \text{ yr}^{-1}$ ). These findings highlight the importance of minimizing temporal inconsistency in long-term vegetation index datasets, which can support more reliable trend analysis in global vegetation response to climate changes.

\* Corresponding author at: Department of Landscape Architecture and Rural Systems Engineering, Seoul National University, Seoul, Republic of Korea.  
E-mail address: [ryuyr77@gmail.com](mailto:ryuyr77@gmail.com) (Y. Ryu).

<https://doi.org/10.1016/j.rse.2024.114282>

Received 7 January 2024; Received in revised form 17 June 2024; Accepted 17 June 2024

Available online 2 July 2024

0034-4257/© 2024 The Authors. Published by Elsevier Inc. This is an open access article under the CC BY license (<http://creativecommons.org/licenses/by/4.0/>).

## 1. Introduction

There has been growing debates on the trend of global vegetation greenness and its relation with climate change (Piao et al., 2020). Many studies have reported global greening since 2000 using various satellite-derived variables including vegetation index, leaf area index (LAI), and solar-induced fluorescence (SIF) (Zhang et al., 2017; Chen et al., 2019; Li and Xiao, 2019), while the long-term trends of those variables since the 1980s are divergent depending on different satellite products (Piao et al., 2020). For example, a recent study reported a sharp declining trend in the global CO<sub>2</sub> fertilization effect on vegetation photosynthesis (Wang et al., 2020). However, subsequent commentary papers raised concerns about technical issues in Advanced Very High-Resolution Radiometer (AVHRR) Near-Infrared Reflectance of vegetation (NIRv) datasets (Frankenberg et al., 2021; Zhu et al., 2021), which is strong proxy of vegetation photosynthesis by minimizing soil background effects (Badgley et al., 2019; Dechant et al., 2020). Frankenberg et al. (2021) reported artifacts in AVHRR NIRv datasets stemmed from inconsistent biases between AVHRR sensors and the orbital drifting effect. Zhu et al. (2021) reported that the harmonized Moderate Resolution Imaging Spectroradiometer (MODIS) NIRv used by Wang et al. (2020) exhibited a smaller greening trend and reduced interannual variations compared to the original MODIS NIRv. These studies showed the importance of rigorous data processing to minimize residual artifacts. Consequently, further steps are imperative in addressing the identified uncertainties including inconsistent bias between different sensors, orbital drifting effect, and inappropriate harmonization across satellites. By examining these artifacts on vegetation index trends, we can gain a more robust understanding of global long-term vegetation dynamics.

Since the early 1980s, the AVHRR sensors on board the National Oceanic and Atmospheric Administration (NOAA) polar-orbiting environmental satellites have provided the longest data records of global satellite measurements on land surface (Pedelty et al., 2007; Franch et al., 2017; Vermote, 2021; Santamaria-Artigas et al., 2021). Long-term AVHRR observations have been widely used to derive vegetation products, including NDVI (Tucker et al., 2005; Pinzon and Tucker, 2014), NIRv (Wang et al., 2020), SIF (Fang et al., 2023), LAI, fraction of photosynthetically active radiation (FPAR) (Myneni et al., 1997; Liu et al., 2012; Zhu et al., 2013; Xiao et al., 2016), and gross primary production (GPP) (Smith et al., 2016; Wang et al., 2021). These AVHRR-based downstream have been widely used in a variety of global ecological studies, such as ecosystem responses to disturbances and long-term climate change. These products have been crucial in understanding the global terrestrial carbon cycle and climate feedbacks (Zhu et al., 2016; Keenan et al., 2016; Chen et al., 2019; Piao et al., 2020).

Relentless efforts have led to considerable improvement in AVHRR vegetation index datasets (Pinzon and Tucker, 2014; Zhu et al., 2013; Xiao et al., 2016). The Global Inventory Modeling and Mapping Studies (GIMMS) NDVI applied Bayesian methods with high-quality NDVI data from the Sea-Viewing Wide Field-of-view Sensor (Pinzon and Tucker, 2014). While GIMMS NDVI had the highest temporal consistency among the different long-term AVHRR-based NDVI datasets, residual orbital drift effects and sensor degradation may lead to temporal inconsistency (Tian et al., 2015). Recently, Li et al. (2023) improved temporal consistency of the GIMMS3g NDVI (PKU GIMMS) by calibrating GIMMS3g NDVI with Landsat and MODIS NDVI. The AVHRR Long-Term Data Record (LTDR) team has provided a high-quality Bi-directional Reflectance Distribution Function (BRDF) normalized daily surface reflectance, which is a unique data source for investigating long-term vegetation index from the spectral reflectance level (Pedelty et al., 2007; Franch et al., 2017; Santamaria-Artigas et al., 2021). In the case of LTDR V3, Nagol et al. (2014) demonstrated that applying a BRDF correction led to a substantial reduction in spurious inter-annual NDVI trends. Franch et al. (2017) reported an improved data quality of LTDR V4 BRDF normalized reflectance with geolocation correction and cloud

mask improvement by evaluating it against in-situ data and MODIS surface reflectance. Enhancements in the LTDR V5 encompassed a BRDF correction, calibration, and atmospheric correction with improved quality assessment flags (Vermote, 2021; <https://landweb.modaps.eosdis.nasa.gov/>). A recent study comprehensively evaluated LTDR V5 spectral reflectance using Landsat-5 surface reflectance and reported enhanced performance with improved BRDF correction (Santamaria-Artigas et al., 2021).

Nevertheless, a number of studies have pointed out remaining issues concerning temporal inconsistency in AVHRR vegetation index datasets (Giglio and Roy, 2020; Zhu et al., 2021; Frankenberg et al., 2021). The first issue contributing to the temporal inconsistency was the inconsistent biases between AVHRR sensors identified at pseudo-invariant calibration sites (PICS). Earlier studies found that inconsistent bias between AVHRR sensors introduced notable temporal inconsistency in spectral reflectance (Latifovic et al., 2012; Li et al., 2014). Recent studies reported residual temporal inconsistency in spectral reflectance and vegetation index across successive AVHRR sensors over desert calibration sites, even with updated retrievals (Giglio and Roy, 2022; Frankenberg et al., 2021). For example, Frankenberg et al. (2021) reported that variations in detrended global AVHRR NIRv were closely similar to those found at PICS locations, suggesting that a major proportion of the variabilities in downstream vegetation indices was caused by spurious instrumental biases instead of true vegetation signal.

The second issue concerns the orbital drifting effects on spectral reflectance and vegetation index. The orbital drifting effect affects changes in the local overpass time of the sensors leading to changes in the solar zenith angle (SZA). This poses an issue, as the surface reflectance over anisotropic surfaces varies depending on the SZA (Fensholt et al., 2009; Nagol et al., 2014; Roy et al., 2020). The orbital drifting effects on spectral reflectance and vegetation index vary depending on ecosystems due to different surface anisotropic characteristics (Gutman, 1999; Los et al., 2005). For example, evergreen needleleaf forest showed a positive relationship between NDVI and SZA due to the larger reduction of red reflectance than near-infrared (NIR) reflectance with increasing SZA, while deciduous broadleaf forest did not show a clear relationship between NDVI and SZA (Deering et al., 1999). Regarding a trend analysis, several studies have reported orbital drifting effects across the different AVHRR-based NDVI products and potential uncertainty in NDVI trends across the latitudes (Tian et al., 2015; Beck et al., 2011). For instance, tropical regions near the equator suffered from orbital drifting effects due to a larger annual SZA anomaly than other regions (Tian et al., 2015). Furthermore, a large annual anomaly of SZA in NOAA 07, 09, 11, and 14 had a more notable orbital drifting effect compared to NOAA 16, 18, 19, and MetOP-B which had relatively smaller SZA annual anomaly (Frankenberg et al., 2021).

The last issue concerns the incomplete harmonization of AVHRR vegetation indices with other satellite products. Because of the broad red and NIR wavelength channels in AVHRR sensors, many studies have tried to harmonize AVHRR NDVI with MODIS NDVI, which is designed to better capture vegetation signals with narrow spectral channels (Chen et al., 2019; Zhu et al., 2021). The spectral response matching method for generating consistent surface reflectance showed good performance in adjustments across AVHRR sensors but showed an insufficient relationship between AVHRR and MODIS (Trishchenko et al., 2002). Other studies have adopted several approaches to harmonize AVHRR with MODIS including pixel-wise linear model (Mao et al., 2012), and cumulative distribution frequency matching (Wang et al., 2020). But further studies showed that non-linearities between different satellite NDVI products limited a global scale application of the linear model-based approach (Ju and Masek, 2016; Berner et al., 2020). For this, studies demonstrated the strength of machine learning-based harmonization for addressing the non-linear relationships between different satellite NDVI products (Berner et al., 2020; Li et al., 2023). Recently, Zhu et al. (2021) showed that an incomplete harmonization of MODIS NIRv with AVHRR NIRv could lead to a large discrepancy in interannual

variations and trends due to the uncertainties in those AVHRR NIRv datasets. Therefore, we should address the ongoing challenges of temporal inconsistency in AVHRR vegetation index datasets for a robust understanding of long-term vegetation trends (Santamaria-Artigas et al., 2021).

In this study, we generated robust NDVI and NIRv datasets based on AVHRR LTDR V5 by addressing temporal inconsistency stemming from inconsistent biases across AVHRR sensors, the orbital drifting effects, and incomplete harmonization with MODIS. We aimed to enhance the temporal consistency of long-term NDVI and NIRv datasets and to investigate how the resulting vegetation trends change.

## 2. Materials and methods

### 2.1. Data

#### 2.1.1. AVHRR LTDR V5

We used the AVHRR LTDR V5 surface reflectance product (AVH09C1) generated from AVHRR L1b Global Area Coverage (GAC) data for 1982–2021 (Franch et al., 2017; Santamaria-Artigas et al., 2021; Vermote, 2021). LTDR V5 used eight satellites including NOAA-07, 09, 11, 14, 16, 18, 19, and MetOP-B from June of 1981 to the present day (Table 1) LTDR V5 provides BRDF normalized reflectance by applying VJB method (Vermote et al., 2008) which has a daily temporal resolution and 0.05° spatial resolution in the Climate Modeling Grid (CMG). We used BRDF normalized reflectance with a fixed solar (SZA: 45°) and viewing geometry (View zenith angle, VZA: 0°) from red (0.58–0.68 μm) and near-infrared (NIR) (0.72–1.10 μm) channels, SZA at overpass time, and quality assessment layer. The detailed relative spectral responses of each AVHRR satellite were in Fig. A1. We only used valid, cloud-free, and BRDF normalized pixels after filtering out low-quality data using the quality flags. The obvious low-quality data at the beginning of the NOAA 11 operating period (1988.11–1989.10) reported by Tian et al. (2015) were replaced with an average of the data from the previous and the subsequent year in each month before applying further processing. Also, it is worth mentioning that while the VJB method can allow a relatively simple BRDF inversion compared to the semi-empirical BRDF model, it has limitations because it assumed a constant BRDF shape throughout the year, and the BRDF parameters were linearly related to NDVI (Vermote et al., 2008). These assumptions of the VJB method may contribute to the remaining orbital drifting effects.

#### 2.1.2. MODIS

We used MODIS BRDF product (MCD43C1, Collection 6.1) distributed by the Land Processes Distributed Active Archive Center (LP DAAC) (Wang et al., 2018) as a reference for generating consistent long-term vegetation index dataset. MCD43C1 have a daily temporal resolution and 0.05° spatial resolution in the CMG grid. MODIS BRDF normalized reflectance with fixed geometry (SZA: 45°; VZA: 0°), consistent with the processed AVHRR data (Section 2.1.1), was computed with high-quality BRDF parameters in MCD43C1 from red (0.62–0.67 μm) and NIR (0.84–0.88 μm) channels (Wang et al., 2018) using semi-empirical RossThick-LiSparse reciprocal BRDF model (Roujean et al., 1992;

**Table 1**  
List of satellites used to process AVHRR LTDR V5 (Vermote, 2021).

Satellite	Start (Year, Day of year)	End (Year, Day of year)
NOAA 07	1982, 001	1985, 003
NOAA 09	1985, 004	1988, 312
NOAA 11	1988, 313	1994, 365
NOAA 14	1995, 001	2000, 305
NOAA 16	2000, 306	2005, 365
NOAA 18	2006, 001	2009, 365
NOAA 19	2010, 001	2016, 366
MetOP-B	2017, 001	2021, 365

Wanner et al., 1995; Schaaf et al., 2002) from February of 2000 to December of 2021.

#### 2.1.3. Pseudo invariant calibration sites (PICS)

To evaluate temporal consistency in spectral reflectance and vegetation index, we used a PICS, which has high temporal stability on surface optical properties (Bacour et al., 2019). In this study, a total of 26 PICS were used for cross-sensor calibration (20 sites) and validation (6 sites), which were registered in U.S. Geological Survey (USGS) radiometric sites catalog ([https://calval.cr.usgs.gov/apps/radsites\\_catalog](https://calval.cr.usgs.gov/apps/radsites_catalog)) and Committee on Earth Observation Satellites (CEOS) (<https://calvalportal.ceos.org/>) (Fig. A2; Table A1). Considering the characteristic of PICS, robust long-term data are expected to have no significant trends and less interannual variability in spectral reflectance and vegetation index at those locations (Latifovic et al., 2012; Zhang et al., 2017; Giglio and Roy, 2020).

### 2.2. Methods

Before applying our three-step post-processing, we calculated monthly 0.05° spectral reflectance (AVHRR<sub>LTDR</sub>) by averaging daily spectral reflectance in each pixel. To fill the remaining data gaps, we introduced a widely used harmonic analysis of time series (HANTS) method using ‘HANTS’ function in MATLAB (Abouali, 2023). Then we calculated monthly NDVI (Tucker, 1979) and NIRv (Badgley et al., 2017) with monthly gap-filled, BRDF normalized NIR and red reflectance.

#### 2.2.1. Cross-sensor calibration

To mitigate the inconsistent bias in surface reflectance among different AVHRR sensors, we conducted cross-sensor calibration using a simple linear regression model. First, we extracted the monthly NIR and red reflectance at 20 calibration PICS (Table A1). We filtered out the outliers with two standard deviations above or below the average values for each instrument, mostly caused by undetected sub-pixel clouds, shadows or haze (Latifovic et al., 2012). Then we calculated averaged monthly NIR and red reflectance in each AVHRR satellite period in each PICS site. We derived the linear regression coefficients between the target spectral reflectance from each AVHRR satellite and the reference spectral reflectance from MetOP-B at each PICS site (Table A1; Table 1). We used spectral reflectance from the latest sensor in the LTDR V5 (MetOP-B) as a reference for cross sensor-calibration because it has reliable sensor characteristics and observation conditions (Santamaria-Artigas et al., 2021). We calculated the cross-calibration factor of each AVHRR satellite by averaging linear regression coefficients in 20 calibration PICS (Table A2). Last, we applied the derived cross-calibration factor of each AVHRR satellite to the original AVHRR<sub>LTDR</sub> spectral reflectance to generate cross-calibrated (AVHRR<sub>cross-calibrated</sub>) spectral reflectance. Six independent validation PICS were used to evaluate the temporal consistency in AVHRR<sub>cross-calibrated</sub> and vegetation indices. AVHRR<sub>cross-calibrated</sub> was calculated with the following equations:

$$\rho_{reference} = m_{ij} \times \rho_{target} \quad (1)$$

$$CF_j = \frac{\sum_{i=1}^{20} m_{ij}}{20} \quad (2)$$

**AVHRR<sub>cross-calibrated</sub> spectral reflectance**

$$= CF \times AVHRR_{LTDR} \text{ spectral reflectance} \quad (3)$$

where  $m$  is slope in the linear regression,  $i$  is index of PICS location,  $j$  is spectral channel (red and NIR band),  $\rho_{reference}$  is the reference spectral reflectance from MetOP-B and  $\rho_{target}$  is the spectral reflectance from each AVHRR satellite (Table 1). CF is cross-calibration factor of each satellite period.

### 2.2.2. Orbital drifting correction

To minimize the orbital drift effects on AVHRR sensors, we applied a second correction to the AVHRR<sub>cross-calibrated</sub> spectral reflectance in each pixel. First, we computed the linear model between the spectral reflectance and SZA at each pixel using entire time-series data. To avoid spurious correlations between spectral reflectance and SZA, we detrended the annual anomalies in both spectral reflectance and SZA. Second, we calculated the orbit-correction factor by applying a linear model to monthly SZA anomalies across the global pixels. Last, we calculated orbit-corrected (AVHRR<sub>orbit-corrected</sub>) spectral reflectance by subtracting the orbit-correction factor from the AVHRR<sub>cross-calibrated</sub> spectral reflectance. Then we evaluated the interannual variability and detrended annual anomaly in AVHRR<sub>LTDR</sub>, AVHRR<sub>cross-calibrated</sub>, and AVHRR<sub>orbit-corrected</sub> spectral reflectance and vegetation index at PICS to assess temporal consistency. AVHRR<sub>orbit-corrected</sub> spectral reflectance was calculated with the following equation:

$$\Delta \text{annual AVHRR}_{\text{cross-calibrated } i} = a_i \times \Delta \text{annual SZA}_i + b_i \quad (4)$$

$$\text{OCF}_i = a_i \times \Delta \text{monthly SZA}_i + b_i \quad (5)$$

$$\begin{aligned} \text{AVHRR}_{\text{orbit-corrected}} \text{Spectral reflectance}_i \\ = \text{AVHRR}_{\text{cross-calibrated}} \text{ spectral reflectance}_i - \text{OCF}_i \end{aligned} \quad (6)$$

where  $i$  is number of global pixels,  $a_i$  is slope in the linear regression,  $b_i$  is intercept,  $\Delta \text{annual AVHRR}_{\text{cross-calibrated } i}$  and  $\Delta \text{annual SZA}_i$  are detrended annual anomalies in spectral reflectance and SZA,  $\Delta \text{monthly SZA}_i$  is monthly anomaly in SZA, and  $\text{OCF}_i$  is orbit-correction factor.

### 2.2.3. Harmonization

To harmonize the AVHRR<sub>orbit-corrected</sub> vegetation indices with MODIS vegetation indices, we applied a two-step harmonization process. We considered the latest version of MODIS vegetation indices (Collection 6.1) as the most reliable and well-validated products (Zhang et al., 2017; Miura et al., 2021; Zhu et al., 2021). The discrepancies in sensor characteristics between AVHRR and MODIS resulted in the different responses of spectral reflectance to atmospheric and surface conditions, which led to differences in vegetation index (Chen et al., 2019; Zeng et al., 2022). To account for those differences in vegetation index, we used additional explanatory variables for considering atmospheric condition (aerosol optical depth and cloud fraction) and surface condition (snow cover and land cover type). The harmonization process consists of a pixel-wise linear model (Mao et al., 2012) and a machine learning-based approach to consider the non-linear relationship between AVHRR<sub>orbit-corrected</sub> and MODIS vegetation indices (Berner et al., 2020). First, we fitted the linear model between the monthly AVHRR<sub>orbit-corrected</sub> NDVI and NIRv and MODIS NDVI and NIRv from 2000 to 2021 at the corresponding pixel and applied it to AVHRR<sub>orbit-corrected</sub> NDVI and NIRv. Second, we generated harmonized vegetation index (AVHRR<sub>harmonized</sub>) using the Cubist regression model (Quinlan, 1992), which can capture non-linearity based on decision trees and rules derived from the training data (Table A4). We trained the model using five input variables including linearly-adjusted AVHRR<sub>orbit-corrected</sub> vegetation index, aerosol optical depth, cloud fraction, snow cover, and land cover type against MODIS vegetation indices. We randomly selected training pixels in odd years and selected the validation pixels in even years from the same overlapping periods for 2000–2021. The Cubist model performed well in both the training ( $R^2 = 0.93\text{--}0.94$ ) and validation ( $R^2 = 0.90\text{--}0.91$ ) (Fig. A5). We used the resampled 0.05°, monthly MERRA-2 aerosol optical depth (Randles et al., 2017), ERA-5 cloud fraction, snow cover data (Hersbach et al., 2020), the MCD12C1 land cover product with the International Geosphere–Biosphere Programme (IGBP) scheme for the period 2001–2021 (Friedl and Sulla-Menashe, 2022), and the European Space Agency Climate Change Initiative (ESA-CCI) land cover product converted into IGBP classes for the period before 2001 (Defourny et al., 2012). Since the ESA-CCI land

cover product was not available for 1982–1991, we used the 1992 data for this period. AVHRR<sub>harmonized</sub> vegetation index was calculated with the following equations:

$$\text{MODIS vegetation index}_i = a_i \times \text{AVHRR}_{\text{orbit-corrected}} \text{vegetation index}_i + b_i \quad (7)$$

$$\begin{aligned} \text{Adj AVHRR}_{\text{orbit-corrected}} \text{vegetation index}_i \\ = a_i \times \text{AVHRR}_{\text{orbit-corrected}} \text{vegetation index}_i + b_i \end{aligned} \quad (8)$$

$$\begin{aligned} \text{AVHRR}_{\text{harmonized}} \text{vegetation index}_i \\ = f(\text{Adj AVHRR}_{\text{orbit-corrected}}, \text{AOD}, \text{CLD}, \text{SNW}, \text{LC})_i \end{aligned} \quad (9)$$

where  $i$  is number of global pixels,  $a_i$  is linear regression coefficient,  $b_i$  is intercept,  $\text{Adj AVHRR}_{\text{orbit-corrected}} \text{vegetation index}_i$  is a linearly-adjusted AVHRR<sub>orbit-corrected</sub> vegetation index. AOD, CLD, SNW, and LC indicate aerosol optical depth, cloud fraction, snow cover, and land cover type, respectively.

### 2.2.4. Statistical analysis

We applied the widely used Mann-Kendall test for calculating long-term trends in vegetation index (Chen et al., 2019). Mann-Kendall test is a non-parametric test for detecting monotonic trends in time series data. We used the ‘pyMannKendall’ python function (Hussain and Mahmud, 2019). We calculated annual growing season vegetation indices by averaging monthly vegetation values with temperature climatology  $\geq 0$  °C using ERA-5 temperature product (Prentice et al., 2011). Then at the pixel level, we computed pixel-wise growing season NDVI and NIRv trends for three different periods including 1982–2021, 1982–1999 and 2000–2021. For global trends, we calculated global NDVI and NIRv by calculating area-weighted averaged values.

To investigate the relative effects of cross-calibration, orbit correction, and harmonization on the trends of the vegetation indices, we quantified the effects of each processing on trends. We defined the effect of each processing on trends as the relative changes in trends between consecutive processing steps: AVHRR<sub>LTDR</sub>–AVHRR<sub>cross-calibrated</sub>, AVHRR<sub>cross-calibrated</sub>–AVHRR<sub>orbit-corrected</sub>, and AVHRR<sub>orbit-corrected</sub>–AVHRR<sub>harmonized</sub>. We would like to note that the uncertainty of each processing step is not entirely independent, so the uncertainty of the first processing step could propagate into the second and third processing steps.

## 3. Results

### 3.1. Evaluation of AVHRR<sub>LTDR</sub> and AVHRR<sub>cross-calibrated</sub> data

We found an enhanced temporal consistency in AVHRR<sub>cross-calibrated</sub> spectral reflectances and vegetation indices compared to AVHRR<sub>LTDR</sub> at PICS (20 sites for calibration and 6 sites for validation) (Fig. 1). Across the PICS, AVHRR<sub>LTDR</sub> NIR reflectance showed a notable decreasing trend, while AVHRR<sub>LTDR</sub> red reflectance had an increasing trend for 1982–2021 (NIR:  $-0.0002 \pm 0.0003 \text{ yr}^{-1}$ ; Red:  $0.0003 \pm 0.0002 \text{ yr}^{-1}$ ). Both AVHRR<sub>LTDR</sub> NDVI and NIRv showed a clear decreasing trend (NDVI:  $-0.0006 \pm 0.0002 \text{ yr}^{-1}$ ; NIRv:  $-0.0003 \pm 0.0001 \text{ yr}^{-1}$ ). After applying cross-calibration, NIR, red reflectance, NDVI, and NIRv showed a reduced trend at both the calibration and validation PICS. The impact of cross-sensor calibration on the AVHRR-2 sensor periods (NOAA 07, 09, 11, and 14) was considerable, whereas the AVHRR-3 sensor periods (NOAA 16, 18, and 19) exhibited relatively minor differences between the original LTDR and cross-calibrated data (Fig. 1; Table A2).

### 3.2. Evaluation of AVHRR<sub>cross-calibrated</sub> and AVHRR<sub>orbit-corrected</sub> data

Our results demonstrated that orbit-drifting correction reduced the

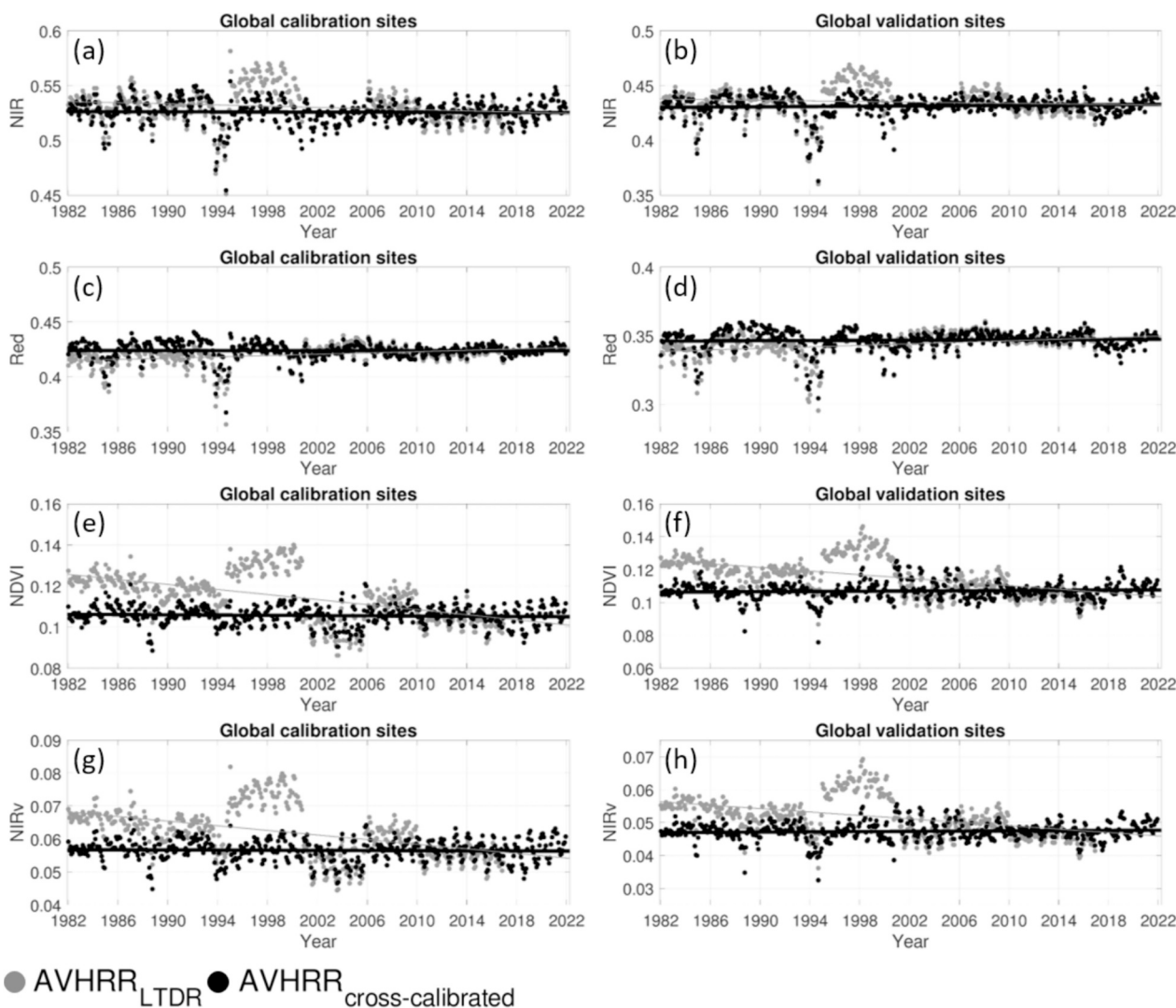


**Fig. 1.** Comparison of averaged cross-calibrated and original LTDR AVHRR NIR (a–b), red reflectance (c–d), NDVI (e–f), and NIRv (g–h) at Pseudo-invariant Calibration Site (PICS) over 1982–2021. A total of 26 PICS were used for calibration (Left panel, 20 sites) and validation (Right panel, 6 sites). Grey dots indicate original LTDR AVHRR data and black dots indicate cross-calibrated AVHRR data. (For interpretation of the references to colour in this figure legend, the reader is referred to the web version of this article.)

temporal inconsistency in AVHRR<sub>cross-calibrated</sub> spectral reflectances and vegetation indices across the PICS (Fig. 2; Fig. A4). We examined the detrended annual anomalies for each processing levels of data. AVHRR<sub>LTDR</sub> spectral reflectance and vegetation indices had a marked temporal inconsistency, whereas both cross-calibrated and orbit-corrected data showed improved temporal consistency throughout the 1982–2021 (Fig. 2). Both cross-sensor calibration and orbit-drifting correction led to a reduction in interannual variability for red, NIR reflectance, NDVI, and NIRv (Fig. A4; Table A3). The interannual variability of spectral reflectance decreased from original LTDR (NIR:  $0.0136 \pm 0.0025$ ; Red:  $0.0086 \pm 0.0039$ ) to cross-calibrated (NIR:  $0.0091 \pm 0.0036$ ; Red:  $0.0078 \pm 0.0044$ ) and further to orbit-corrected (NIR:  $0.0083 \pm 0.0036$ ; Red:  $0.0071 \pm 0.0045$ ) data. NDVI and NIRv also showed a reduced interannual variability in cross-calibrated (NDVI:  $0.0057 \pm 0.0025$ ; NIRv:  $0.0029 \pm 0.0009$ ) and orbit-corrected (NDVI:  $0.0055 \pm 0.0020$ ; NIRv:  $0.0027 \pm 0.0007$ ) data compared to the LTDR NDVI and NIRv (NDVI:  $0.0090 \pm 0.0027$ ; NIRv:  $0.0056 \pm 0.0012$ ). Furthermore, the orbit-drifting effect was strongest when the SZA changed abruptly, especially in 1994 (Fig. 2). In addition, the relationships between SZA-NDVI and SZA-NIRv at PICS showed that processing in the order of cross-calibration before orbit correction resulted in nearly

zero correlation coefficients and slightly higher  $p$ -values than the reverse processing order. This finding supported that the cross-calibration among different AVHRR sensors needs to be applied first to minimize the orbital drift effects (Fig. S1).

### 3.3. Evaluation of AVHRR<sub>orbit-corrected</sub> and AVHRR<sub>harmonized</sub> data

We found that the harmonization with MODIS also effectively reduced the residual temporal inconsistency in AVHRR<sub>orbit-corrected</sub> vegetation indices (Fig. 3). Our results showed a weakened interannual variability and trend in AVHRR<sub>harmonized</sub> vegetation indices compared to AVHRR<sub>orbit-corrected</sub> vegetation indices at PICS (Fig. 3). Globally, both AVHRR<sub>harmonized</sub> NDVI and NIRv showed a strong temporal relationship with MODIS NDVI and NIRv during the overlapping period (Fig. 4). The AVHRR<sub>harmonized</sub> NDVI and NIRv showed a consistent seasonal pattern with MODIS NDVI and NIRv across latitudes and plant functional types, including tropical regions for 2000–2021 (Fig. 5; Fig. S3). The spatial distribution of AVHRR<sub>harmonized</sub> NDVI and NIRv trends also well matched with MODIS during the overlapping period (Fig. 6; NDVI: 89.3%; NIRv: 89.5%). We found that the pixels with disagreeing trends between AVHRR<sub>harmonized</sub> and MODIS vegetation indices were

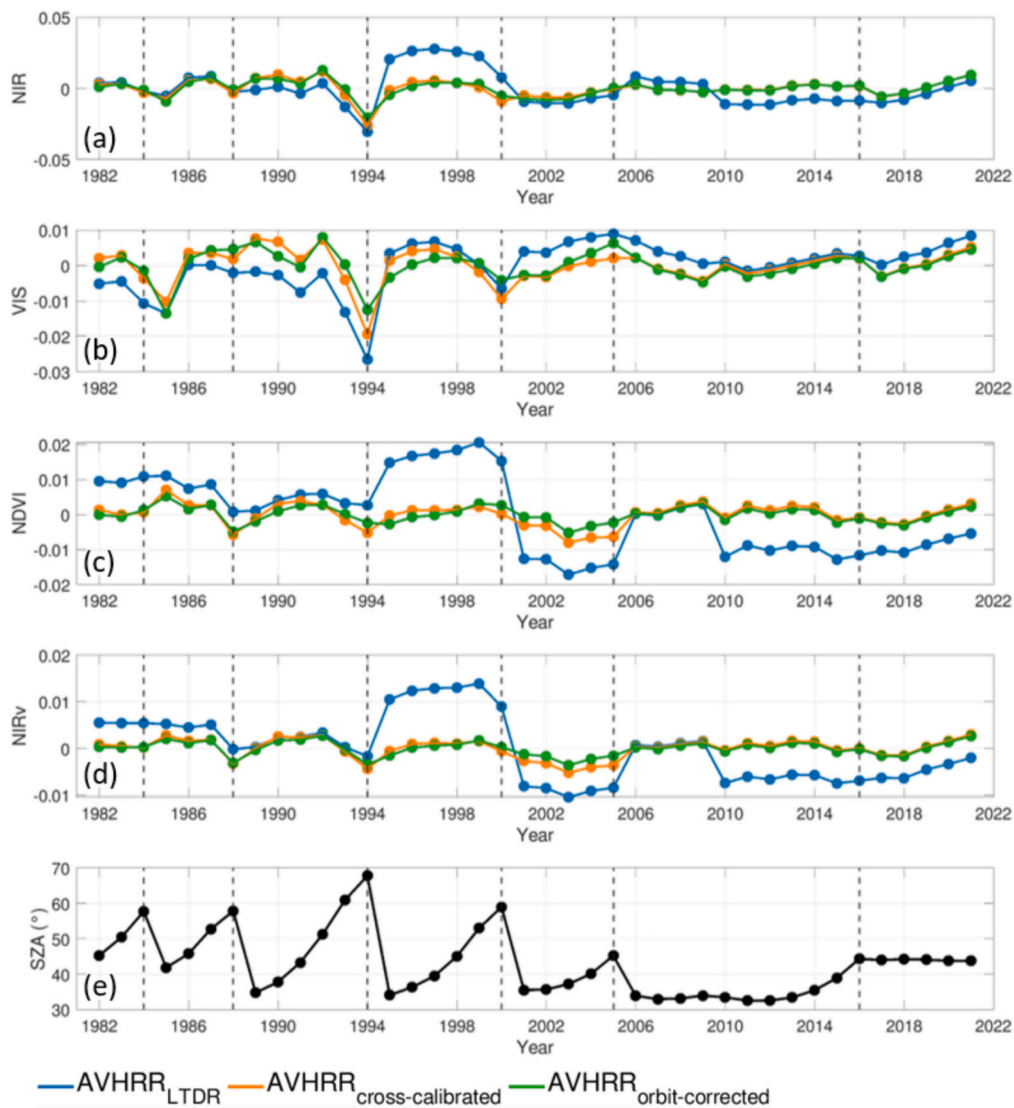


**Fig. 2.** Comparison of detrended anomalies in original LTDR, cross-calibrated, and orbit-corrected AVHRR spectral reflectances (a-b) and vegetation indices (c-d) at Pseudo-invariant Calibration Site (PICS) sites over 1982–2021. Blue dotted lines are LTDR, orange dotted lines are cross-calibrated, and green dotted lines are orbit-corrected annual averaged AVHRR data, respectively. Black dotted lines indicate the annual averaged solar zenith angle at PICS. (For interpretation of the references to colour in this figure legend, the reader is referred to the web version of this article.)

distributed sparsely rather than appearing in a specific region or ecosystem. Furthermore, the AVHRR<sub>harmonized</sub> NDVI and NIR<sub>v</sub> agreed well with MODIS NDVI and NIR<sub>v</sub> across the FLUXNET sites (Fig. S2; Table S1).

### 3.4. Comparison of NDVI and NIR<sub>v</sub> trends with different processing levels

We found that the global long-term trends in NDVI and NIR<sub>v</sub> with four different processing levels differed considerably (Fig. 7). All of NDVI and NIR<sub>v</sub> products in different processing levels showed significant increasing trend. The original AVHRR<sub>LTDR</sub> had similar trends with AVHRR<sub>harmonized</sub>, but the interannual variability of AVHRR<sub>LTDR</sub> had three times larger in NDVI and four times larger in NIR<sub>v</sub> than AVHRR<sub>harmonized</sub>. The interannual variability in NDVI and NIR<sub>v</sub> were gradually reduced as we conducted each processing. We also investigated the trends of each processing level separately for 1982–1999 and 2000–2021 (Fig. 8). Compared to AVHRR<sub>harmonized</sub>, AVHRR<sub>LTDR</sub> NDVI and NIR<sub>v</sub> showed stronger greening trends during 1982–1999 (NDVI: AVHRR<sub>LTDR</sub>: 0.0017 y<sup>-1</sup>; AVHRR<sub>harmonized</sub>: 0.0008 y<sup>-1</sup>; NIR<sub>v</sub>: AVHRR<sub>LTDR</sub>: 0.0008 y<sup>-1</sup>; AVHRR<sub>harmonized</sub>: 0.0003 y<sup>-1</sup>), while the

AVHRR<sub>LTDR</sub> NDVI and NIR<sub>v</sub> exhibited a weakened greening trend during 2000–2021 (NDVI: AVHRR<sub>LTDR</sub>: 0.0005 y<sup>-1</sup>; AVHRR<sub>harmonized</sub>: 0.0008 y<sup>-1</sup>; NIR<sub>v</sub>: AVHRR<sub>LTDR</sub>: 0.0001 y<sup>-1</sup>; AVHRR<sub>harmonized</sub>: 0.0003 y<sup>-1</sup>). The proportion of statistically significant greening trend pixels ( $p < 0.1$ ) decreased as the processing progressed from AVHRR<sub>LTDR</sub>, AVHRR<sub>cross-calibrated</sub>, and AVHRR<sub>orbit-corrected</sub> to AVHRR<sub>harmonized</sub> for 1982–1999, while the proportion of significantly greening trend pixels increased as the processing progressed for 2000–2021 in both NDVI and NIR<sub>v</sub> (Fig. A6; Table A5).

By investigating at the relative effects of cross-calibration, orbit correction, and harmonization on the trends in vegetation indices, we found that the processing having the dominant effect varied from earlier AVHRR satellites (1982–1999) to later AVHRR satellites (2000–2021) (Fig. 9). During the early period from 1982 to 1999, the orbital drifting correction had a dominant impact on the long-term vegetation index trends particularly around the equator (NDVI: Cross-calibration: 19.1%; Orbit correction: 53.2%; Harmonization: 27.7%; NIR<sub>v</sub>: Cross-calibration: 12.9%; Orbit correction: 57.3%; Harmonization: 29.8%). Orbit correction had a notable effect near the equator, where a larger SZA anomaly was observed compared to other regions (Fig. A3). The



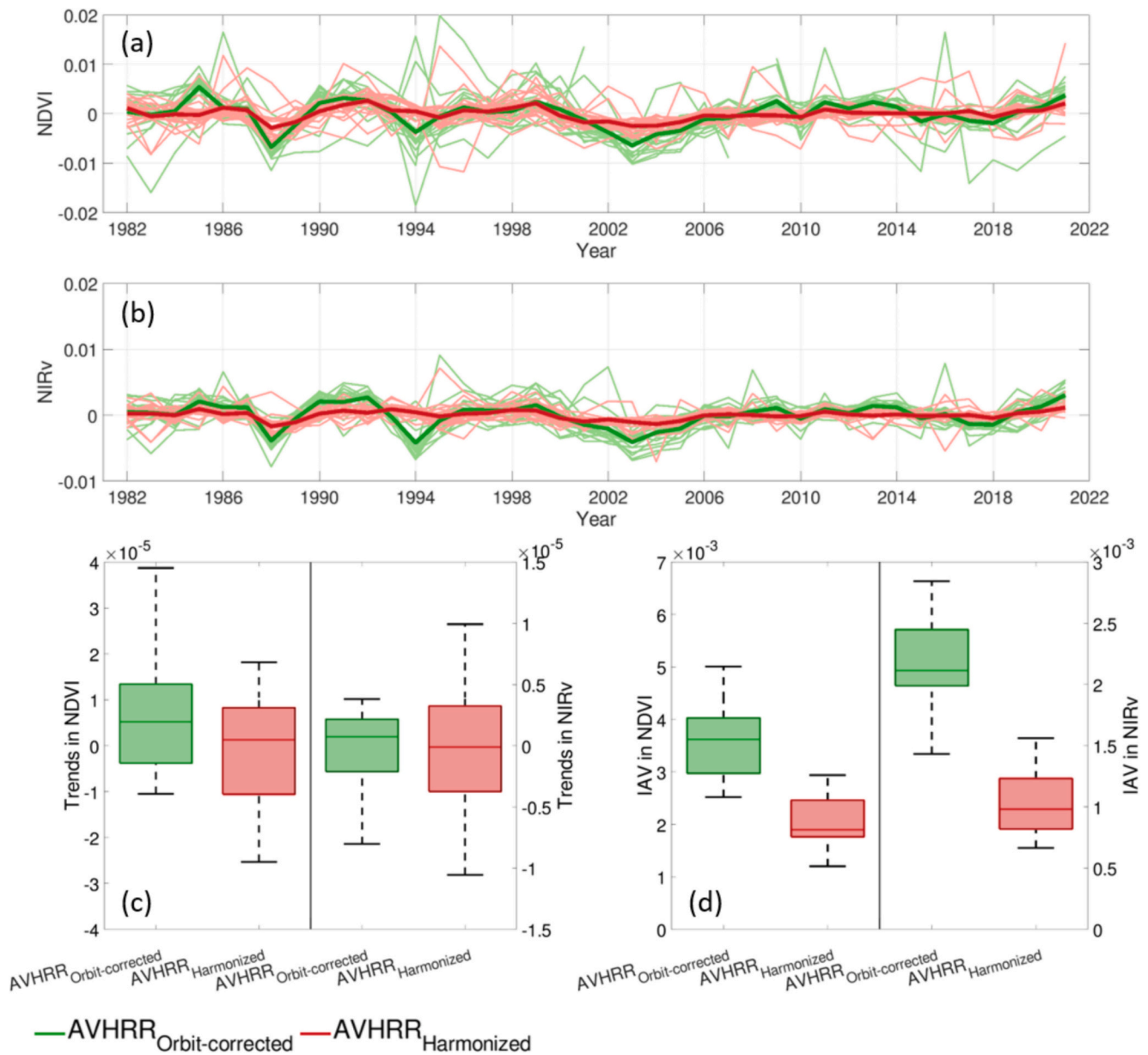


**Fig. 3.** Comparison of detrended anomalies (a-b), trends (c), and interannual variability (d) in orbit-corrected AVHRR and harmonized AVHRR data at Pseudo-invariant Calibration Site (PICS) sites over 1982–2021. Thick lines in (a) and (b) are averaged detrended anomalies. The different colors represent orbit-corrected (green) and harmonized (red), respectively. (For interpretation of the references to colour in this figure legend, the reader is referred to the web version of this article.)

harmonization also showed a considerable effect on long-term trends in NDVI and NIRv, especially in the northern hemisphere. For 2000–2021, relative effects of cross-calibration, orbit correction, and harmonization on global long-term trends in NDVI (Cross-calibration: 35.6%; Orbit correction: 31.3%; Harmonization: 33.1%) and NIRv (Cross-calibration: 35.7%; Orbit correction: 30.9%; Harmonization: 33.4%) exhibited comparable ratios. Across latitudes, the harmonization had a relatively greater impact on both NDVI and NIRv than the other two processing steps in the high-latitude regions.

#### 4. Discussion

##### 4.1. Addressing temporal inconsistency in the long-term AVHRR dataset

Our study demonstrated that cross-calibration across sensors could correct the inconsistent biases in spectral reflectance and vegetation

index between AVHRR sensors at PICS (Fig. 1). We found that sensor cross-calibration systematically reduced the temporal inconsistency across satellites, such as during the NOAA 14 periods which were reported to have a higher bias of NIR reflectance compared to other NOAA satellite periods (Santamaria-Artigas et al., 2021; Frankenberg et al., 2021). Furthermore, we found a noteworthy decreasing trend in AVHRR<sub>LTD</sub> NDVI and NIRv, including at PICS, which were attributed to the decreased trend in NIR reflectance and an increased trend in red reflectance (Fig. 1). After applying cross-calibration to AVHRR<sub>LTD</sub> spectral reflectance, the trend bias in the both AVHRR<sub>LTD</sub> spectral reflectance and vegetation indices were removed. In a previous study, Latifovic et al. (2012) reported cross-calibration could enhance temporal consistency in BRDF normalized reflectance from NOAA 07 to NOAA 19 at eight PICS. Li et al. (2014) also reported the improved temporal consistency of AVHRR top-of-atmosphere reflectance after cross-sensor calibration. Our results highlighted the robustness of the sensor cross-

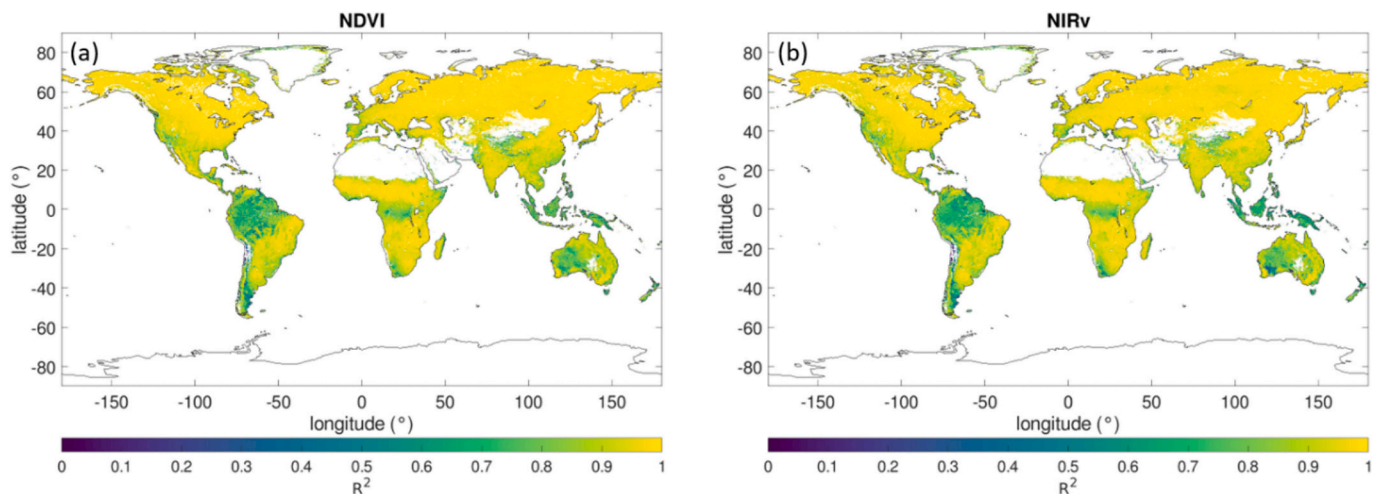


Fig. 4. Spatial distribution of coefficient of determination ( $R^2$ ) between monthly harmonized AVHRR and MODIS NDVI (a) and NIRv (b) for 2000–2021. Statistically significant trends (Mann–Kendall test,  $p < 0.1$ ) are colour-coded. Statistically insignificant pixels and non-vegetated pixels are marked with white colour.

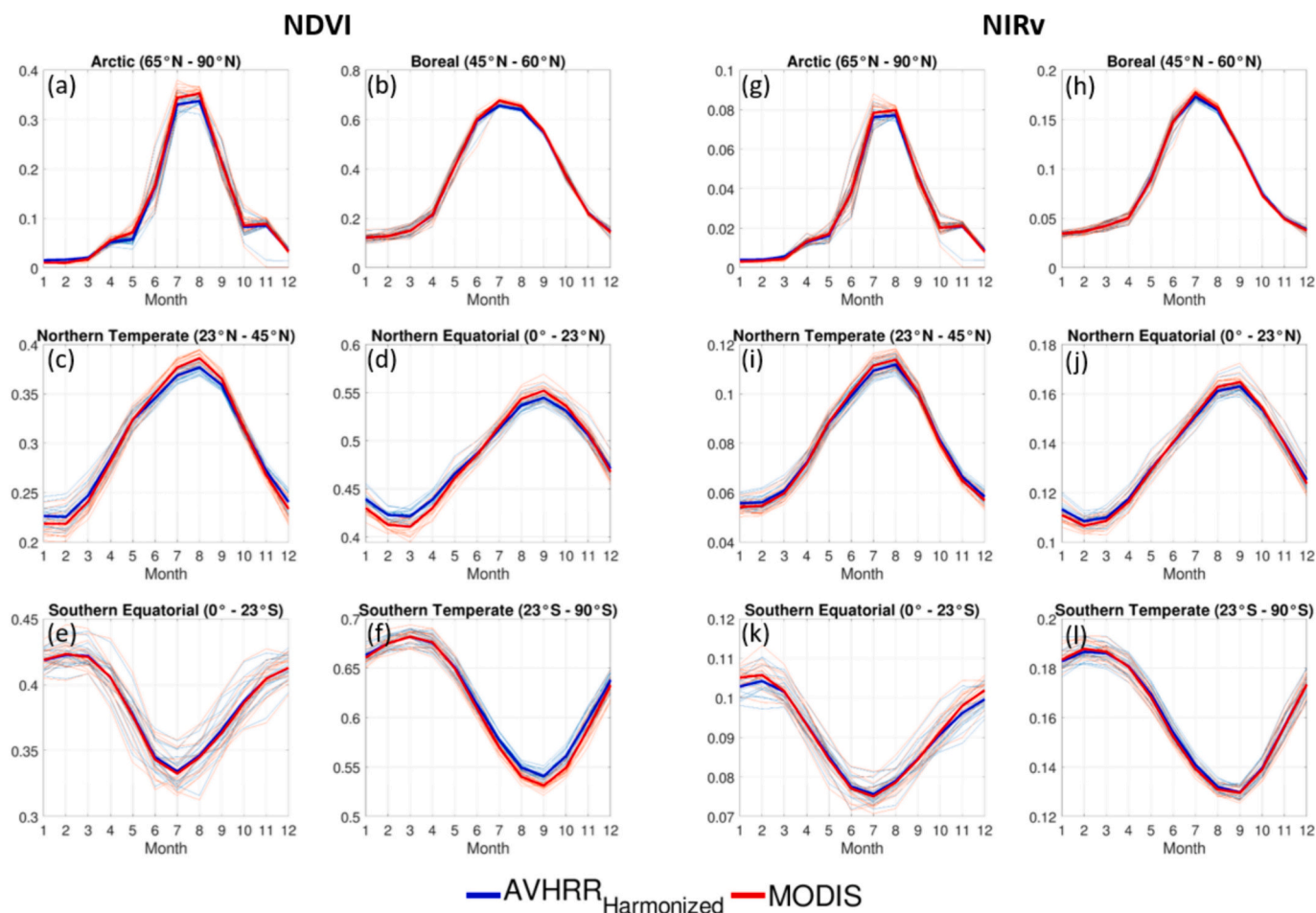
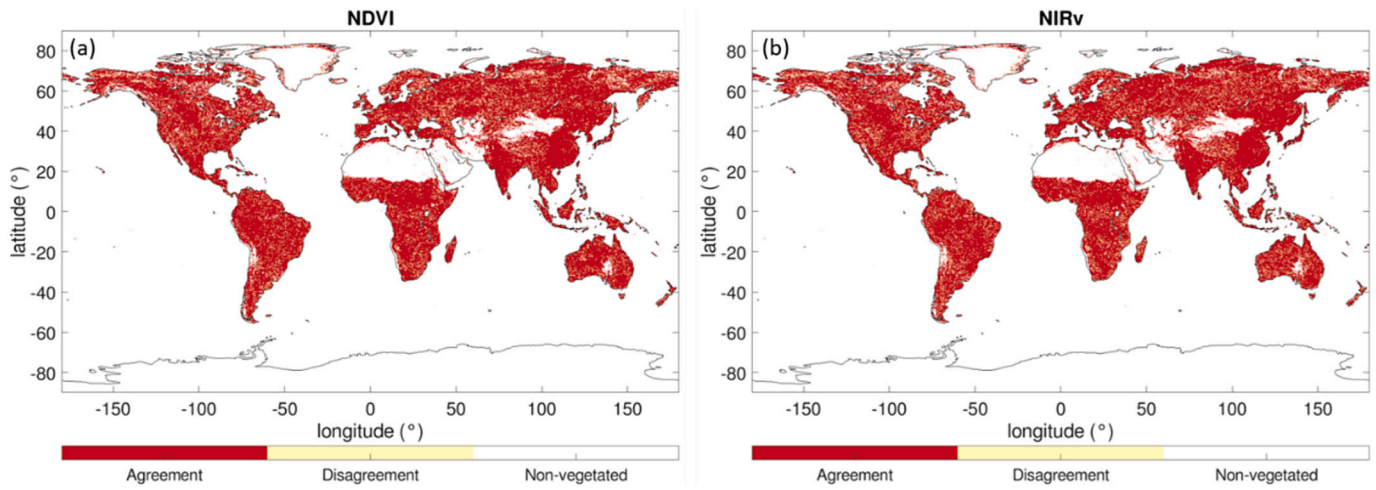


Fig. 5. Comparison of seasonal pattern between harmonized AVHRR (Blue) (a–f) and MODIS (Red) (g–l) NDVI and NIRv. The thin lines indicate a seasonal pattern in each year for 2000–2021 and the thick lines indicate an averaged seasonal pattern. (For interpretation of the references to colour in this figure legend, the reader is referred to the web version of this article.)

calibration approach in reducing temporal inconsistency over an extended validation period and a larger number of PICS (Fig. 1; Table A1).

Our results also presented the significance of orbital drifting correction for decreasing interannual variability artifacts in spectral

reflectance and vegetation indices (Fig. 2; Fig. A4). We found a strongly improved temporal consistency, especially in 1994, which before correction showed the largest anomaly in AVHRR<sub>LTDR</sub> and AVHRR<sub>Cross-calibrated</sub> data across the PICS and global scale due to the largest SZA anomaly (Fig. 2; Fig. 7). These findings can help to enhance our



**Fig. 6.** Spatial distribution of agreements between harmonized AVHRR and MODIS NDVI (a) and NIRv (b) for 2000–2021. Red, yellow, and white colour indicate agreement, disagreement, and non-vegetated pixels, respectively. (For interpretation of the references to colour in this figure legend, the reader is referred to the web version of this article.)

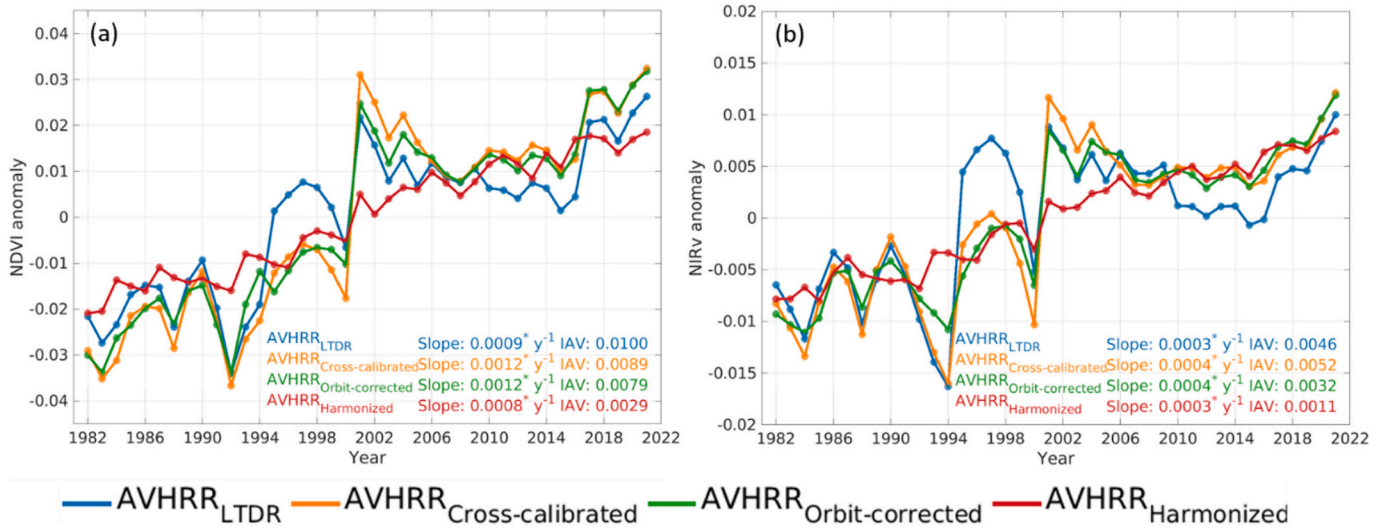


**Fig. 7.** Temporal dynamics in global long-term AVHRR NDVI (a) and NIRv (b) with different processing levels. The different colors represent original LTDR (blue), cross-calibrated (orange), orbit-corrected (green), and harmonized (red) NDVI and NIRv, respectively. (For interpretation of the references to colour in this figure legend, the reader is referred to the web version of this article.)

understanding of the interannual variation in NDVI and NIRv by reducing the artifacts from orbital drifting. We also found that the orbital drifting effects on NIRv were doubled compared to NDVI (NDVI:  $-3.5\%$ ; NIRv:  $-6.9\%$ ) at PICS (Fig. A4). The higher sensitivity of NIRv to the angular effects owing to the NIR reflectance (Zeng et al., 2022; Jeong et al., 2023) can explain the larger orbital drifting effects.

We further demonstrated the importance of harmonization with MODIS for minimizing the temporal inconsistency in AVHRR<sub>orbit-corrected</sub> NDVI and NIRv. The reduced trends and interannual variability in AVHRR<sub>harmonized</sub> vegetation index at PICS provided compelling evidence that the harmonization improved capability of AVHRR data for capturing vegetation changes better with harmonization (Fig. 3). In particular, AVHRR<sub>harmonized</sub> vegetation indices showed good agreement with MODIS vegetation indices across the FLUXNET sites (Fig. S2; Table S1) and did not show spatial bias with MODIS vegetation indices trends across latitudes (Fig. 6). This finding further supports the robustness of the two-step harmonization approach (Berner et al., 2020). In addition, AVHRR<sub>harmonized</sub> vegetation indices showed a similar

interannual variability with MODIS at the global scale (Fig. A8). In contrast with recent studies, which showed significant differences in interannual variability after applying a cumulative distribution frequency matching approach (Zhu et al., 2021; Wang et al., 2021). These findings improve the reliability of trends and interannual variability in the AVHRR<sub>harmonized</sub> vegetation index datasets.

#### 4.2. Global trends in vegetation index with enhanced temporal consistency

Our results revealed a persistent greening trend in AVHRR<sub>harmonized</sub> NDVI and NIRv for 1982–2021. This is notably different from previous studies which showed rapid greening trends in NIRv before 2000 followed by a relatively weakened trend after 2000 (Wang et al., 2020; Zhu et al., 2021). These discrepancies in vegetation index trends can be explained as being due to the unresolved temporal inconsistencies in earlier datasets which led to an overestimated greening trend before 2000 and underestimated greening trend after 2000.

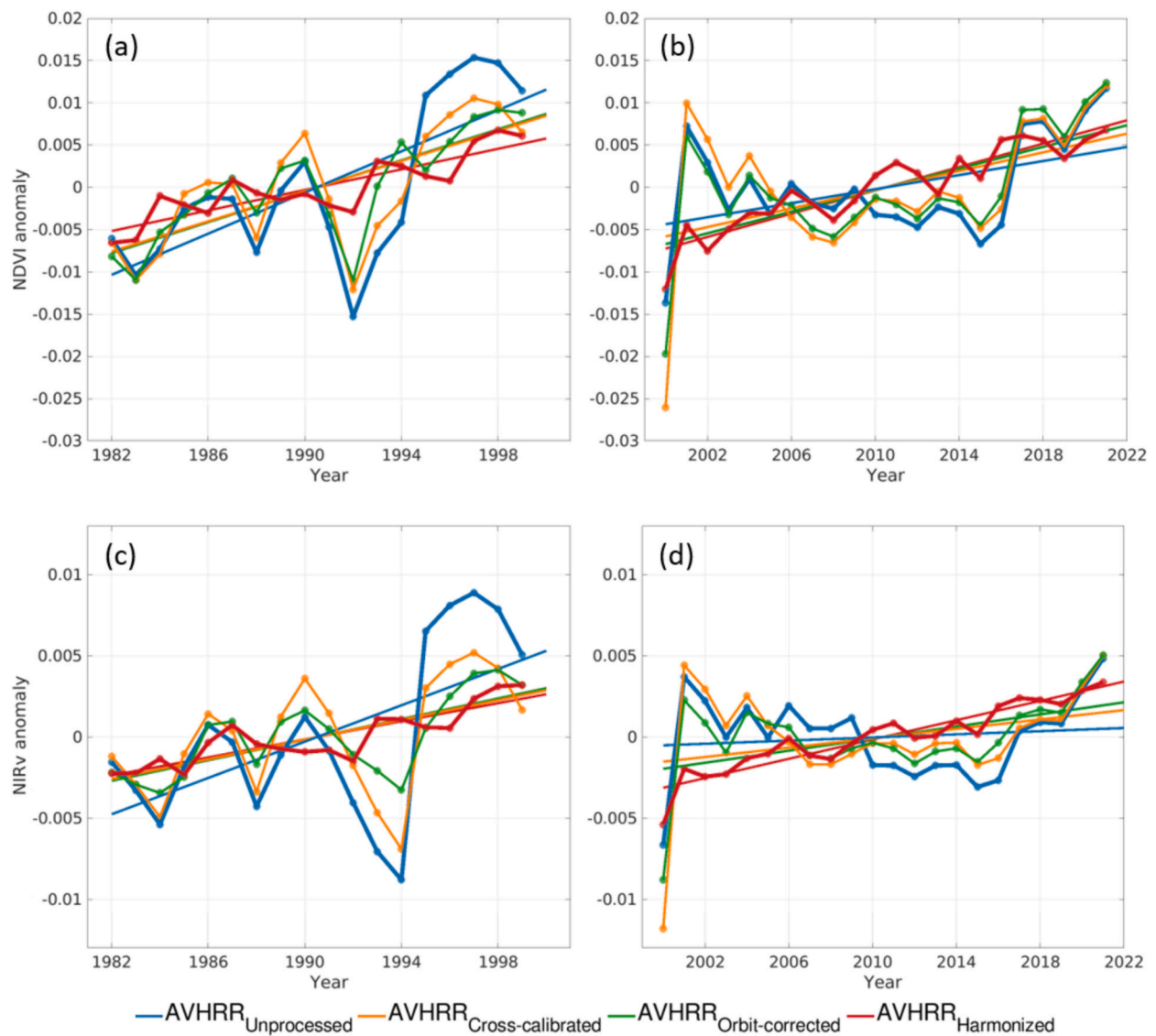


**Fig. 8.** Annual anomalies in different processing levels of long-term AVHRR NDVI (a-b) and NIRv (c-d) for 1982–1999 and 2000–2021. The different colors represent original LTDR (blue), cross-calibrated (orange), orbit-corrected (green), and harmonized (red) NDVI and NIRv, respectively. (For interpretation of the references to colour in this figure legend, the reader is referred to the web version of this article.)

Based on earlier studies, we provided evidence that the global greening trend in NDVI and NIRv might be overestimated for 1982–1999. First, we found that varying biases between AVHRR sensors in AVHRR<sub>LTDR</sub> NDVI and NIRv can lead to an overestimation of the global greening trends for 1982–1999 (Fig. 1; Fig. 8). We found the primary source of an overestimated global greening trend before 2000 was the high bias in the NOAA 14 satellite LTDR NIR reflectance (Fig. 8). The strong AVHRR<sub>LTDR</sub> NIRv trend before 2000 was consistent with a recent study (Wang et al., 2020; Zhu et al., 2021) which used NIRv derived from GIMMS3g NDVI and LTDR V5 NIR reflectance. As GIMMS3g NDVI did not show a noticeably higher global NDVI anomaly during the NOAA 14 period (Tian et al., 2015), we assumed that the AVHRR<sub>LTDR</sub> NIR reflectance data was the primary driver of the observed greening before 2000. We also found that the orbit drifting effects can induce an overestimation of NDVI and NIRv trends for 1982–1999. Following the latitudinal gradient of SZA changes (Fig. A3), the orbit correction also showed stronger effects on the trends in vegetation indices near the equator (Fig. 9). This is supported by, a recent study reported severe orbital drifting effects on GIMMS3g NDVI in tropical evergreen broadleaf forest regions near the equator before 2000 (Li

et al., 2023). They reported negative bias in NOAA 9 NDVI and positive bias in NOAA 11 and 14 NDVI which can cause of overestimation of the greening trend in NDVI before 2000. We found that after addressing the temporal inconsistencies in NDVI datasets, Amazon evergreen broadleaf forests did not show such a strong greening trend and interannual variability for 1982–1999 (Fig. A9). It is suggested that tropical evergreen broadleaf forests contributed the most to the uncertainty of global vegetation trends (Wang et al., 2022). In light of this, the PKU GIMMS NDVI also showed a much-reduced global greening trend and interannual variation before 2000 compared to GIMMS3g NDVI (Li et al., 2023). A reduced greening trend with enhanced temporal consistency in both refined NDVI products supported an overestimated greening trend in 1982–1999. Therefore, future studies need to investigate the greening or browning trends and interannual variability further and their drivers during 1980–1990s using novel datasets with enhanced temporal consistency.

In contrast to 1982–1999, the global greening trend based on NDVI and NIRv can be underestimated after 2000. Overall, we found that a sharply declining AVHRR<sub>LTDR</sub> NDVI and NIRv in early 2000s largely impacted on the trend analysis post 2000, which is not presented in the

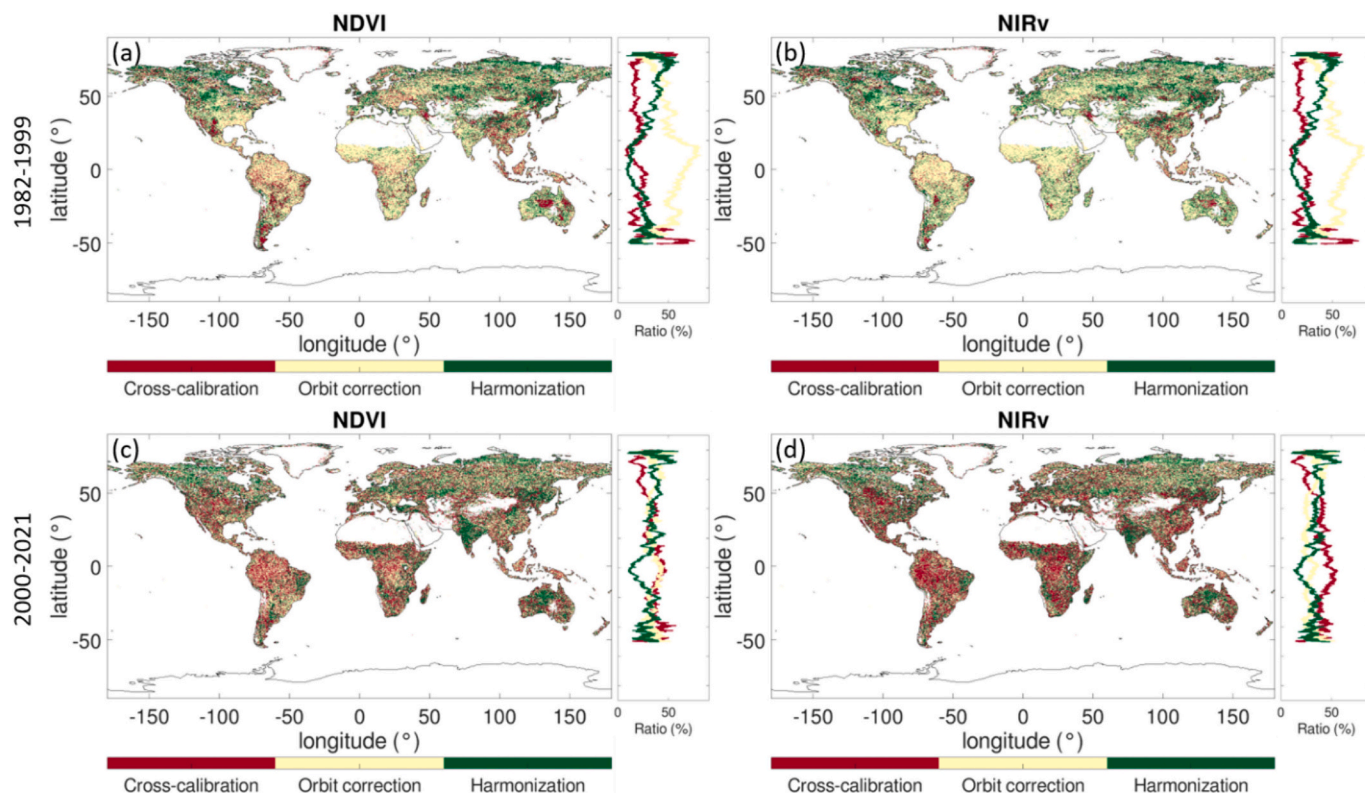


**Fig. 9.** Comparison of the relative three processing effects on long-term trends in NDVI and NIRv for 1982–1999 and 2000–2021. The largest effects of processing were marked followed colors: cross-calibration (red), orbit correction (yellow), and harmonization (green). (For interpretation of the references to colour in this figure legend, the reader is referred to the web version of this article.)

MODIS vegetation indices. This bias was corrected progressively by conducting each processing step. First, we found a considerable inconsistent bias in AVHRR<sub>LTD</sub>R NDVI and NIRv early 2000s. We can expect larger calibration effects before 2000 considering that the AVHRR-2 sensors suffered from sensor degradation while AVHRR-3 sensors had a relatively stable performance (Los, 1998; Bhatt et al., 2016; Chen et al., 2019). But we found that NOAA 16 and 18 also had a substantial inconsistent bias (Fig. 1), and it makes considerable effects on NDVI and NIRv trends compared to orbit correction and harmonization during 2000–2021 (Fig. 9). The orbital drifting effects can lead to an underestimation of the greening trends in vegetation indices. At the global scale, orbit correction led to a considerable increasing greening trend in NDVI and NIRv for 2000–2021 (Fig. 8; Table A5). This result agrees with recent findings. While GIMMS3g showed a weak global greening trend after 2000, PKU GIMMS NDVI showed a strong global trend (Li et al., 2023). Last, AVHRR-MODIS harmonization notably affected NDVI and NIRv trends in the high-latitude regions after 2000. We may explain the higher harmonization effect in the high-latitude regions related to the difference in spectral resolution of the NIR band between AVHRR and MODIS (Fig. A1). The narrow MODIS NIR spectral band can tightly focus on vegetation reflectance. On the other hand, the broader AVHRR NIR band can dilute the signal from increasing vegetation fraction due to the larger water vapor absorption and soil interference (Gitelson and Kaufman, 1998; Van Leeuwen et al., 2006; Brown et al., 2006). Furthermore, we found a consistent greening trend between AVHRR<sub>Rharmonized</sub> and high spatial resolution Landsat NDVI at high-latitude regions including tundra and boreal ecosystems after 2000 (Berner et al., 2020; Fig. A7). As a result, addressing ongoing challenges of temporal inconsistency led to an increased global greening trend after 2000 in both refined AVHRR<sub>Rharmonized</sub> and PKU GIMMS NDVI products compared to their original products. Those findings emphasize the significance of addressing technical issues and biases when harmonizing products of long-term vegetation index datasets to improve the

reliability of trend analysis.

#### 4.3. Implications for future studies

Potential users of this dataset need to consider the assumptions underlying our long-term NDVI and NIRv data production. First, the intrinsic differences of wavelength characteristics, sensor calibration, orbit maintenance between AVHRR and MODIS can have a substantial impact on the vegetation index values and trends (Chen et al., 2019; Zeng et al., 2022). This study used MODIS Collection 6.1 as a validated benchmark dataset for generating long-term NDVI and NIRv, but further improvements in the benchmark datasets could lead to a difference in long-term trends. For example, Zhang et al. (2017) reported a significant global browning trend in MODIS Collection 5 due to the sensor degradation while MODIS Collection 6 vegetation indices, which fixed the sensor degradation issue, showed a greening trend. Second, we assumed that inland water did not substantially affect NDVI and NIRv trends, considering no clear trends in global inland water areas and their small proportion of total land areas (Pickens et al., 2020). Last, MODIS Terra and Aqua are close to being decommissioned and suffered from orbital drifting (<https://terra.nasa.gov/about/terra-orbit-changes>). Future studies need to consider incorporating VIIRS in our proposed approach for generating a long-term vegetation index, while MODIS-VIIRS calibration also should be applied carefully (Fan and Liu, 2016).

#### 5. Summary and conclusion

We developed a new vegetation product with enhanced temporal consistency in long-term NDVI and NIRv after applying a three-step post processing including cross sensor-calibration between AVHRR sensors, orbital drifting correction among AVHRR sensors, and a machine-learning based harmonization with MODIS. Our refined NDVI and NIRv dataset identified a persistent global greening trend over the last

four decades. This finding contrasts with the original LTDR V5 NDVI and NIRv, which exhibited strong greening trends prior to 2000 and diminished greening trends after 2000 stemming from the temporal inconsistency. Overall, our results highlight the critical need for reducing the temporal inconsistency within vegetation index datasets and its substantial impact on long-term trends. We believe that these findings can strengthen our understanding of global long-term vegetation dynamics.

#### CRedit authorship contribution statement

**Sungchan Jeong:** Visualization, Validation, Methodology, Investigation, Formal analysis, Data curation, Conceptualization, Writing – review & editing, Writing – original draft. **Youngryel Ryu:** Supervision, Resources, Project administration, Investigation, Funding acquisition, Conceptualization, Writing – review & editing, Writing – original draft. **Pierre Gentine:** Methodology, Investigation, Conceptualization, Writing – review & editing, Writing – original draft. **Xu Lian:** Methodology, Formal analysis, Writing – review & editing, Writing – original draft. **Jianing Fang:** Investigation, Formal analysis, Conceptualization, Writing – review & editing, Writing – original draft. **Xing Li:** Methodology, Formal analysis, Conceptualization, Writing – review & editing, Writing – original draft. **Benjamin Dechant:** Investigation, Formal analysis, Conceptualization, Writing – review & editing, Writing – original draft. **Juwon Kong:** Formal analysis, Conceptualization, Writing – review & editing, Writing – original draft. **Wonseok Choi:** Investigation, Formal analysis, Writing – review & editing, Writing – original draft. **Chongya Jiang:** Methodology, Investigation, Formal analysis, Data curation, Conceptualization, Writing – review & editing, Writing – original draft. **Trevor F. Keenan:** Investigation, Formal analysis, Conceptualization, Writing – review & editing, Writing – original draft. **Sandy P. Harrison:** Supervision, Resources, Writing – review & editing, Writing – original draft. **Iain Colin Prentice:** Supervision, Resources, Writing – review & editing, Writing – original draft.

## Appendix A. Appendix

**Table A1**  
List of Pseudo Invariant Calibration Site (PICS).

Name	Latitude	Longitude
Arabia 2	20.19°	51.63°
Sudan 1	22.11°	28.11°
Arabia 1	19.80°	47.07°
Egypt 1	26.61°	26.22°
Libya 3	23.22°	23.23°
Libya 2	25.08°	20.77°
Algeria 3	30.63°	7.83°
Mauritania 1	19.51°	−8.57°
Mali 1	19.14°	−5.77°
Libya 4	28.67°	23.42°
Niger 1	20.26°	9.64°
Algeria 1	23.83°	−0.76°
Mauritania 2	19.78°	−8.89°
Algeria 4	29.99°	5.10°
Libya 1	24.65°	13.25°
Algeria 5	31.16°	2.24°
Algeria 2	25.99°	−0.62°
Niger 2	21.33°	10.60°
Niger 3	21.51°	7.86°
Arabia 3	28.80°	43.05°
Taklamakan Desert	39.83°	80.17°
Railroad Valley Playa	38.50°	115.69°
Sonoran Desert	32.35°	114.65°
Dunhuang	40.13°	94.34°
Namib Desert 1	−24.98°	15.27°
Namib Desert 2	−17.33°	12.05°

#### Declaration of competing interest

The authors declare that they have no known competing financial interests or personal relationships that could have appeared to influence the work reported in this paper.

#### Data availability

The refined global long-term AVHRR NDVI and NIRv datasets are available in this link (<https://www.environment.snu.ac.kr/data/longterm-vi>).

#### Acknowledgement

We extend our gratitude to the NASA LTDR team for providing the LTDR V5 products, the MODIS team for the MODIS BRDF products, and the GIMMS team for sharing the GIMMS3g NDVI dataset. This study was supported by National Research Foundation of Korea (RS-2024-00348585). S.J. and W.C. were supported by Knowledge-based Environmental Specialized Graduate Program through the Korea Environmental Industry & Technology Institute (KEITI) funded by the Ministry of Environment (MOE). S.J., Y.R., P.G., X.L. (SNU), J.F., X.L. (Columbia), T.F.K, S.P.H., and I.C.P were supported by the LEMONTREE (Land Ecosystem Models based On New Theory, observations and Experiments) project, funded through the generosity of Eric and Wendy Schmidt by recommendation of the Schmidt Futures program. B.D. was supported by sDiv, the Synthesis Centre of the German Centre for Integrative Biodiversity Research (iDiv) Halle-Jena-Leipzig (DFG FZT 118, 202548816). T.F.K. acknowledged support from a DOE Early Career Research Program award #DE-SC0021023 and NASA Awards 80NSSC21K1705 and 80NSSC20K1801.

**Table A2**

Mean linear regression coefficients between the target spectral reflectance in each AVHRR satellite period and reference spectral reflectance from MetOP-B at the 20 calibration PICS.

Satellite	Slope		R <sup>2</sup>	
	Red-band	NIR-band	Red-band	NIR-band
NOAA-07	1.021	0.990	0.974	0.970
NOAA-09	1.011	0.989	0.950	0.968
NOAA-11	1.015	0.996	0.988	0.961
NOAA-14	0.998	0.953	0.977	0.985
NOAA-16	0.996	1.009	0.949	0.980
NOAA-18	0.992	0.981	0.921	0.985
NOAA-19	1.001	1.011	0.987	0.990

**Table A3**

Interannual variability at PICS.

Name	LTDR	Cross-calibrated	Orbit-corrected
NIR reflectance	0.0136 ± 0.0025	0.0091 ± 0.0036	0.0083 ± 0.0036
Red reflectance	0.0086 ± 0.0039	0.0078 ± 0.0044	0.0071 ± 0.0045
NDVI	0.0090 ± 0.0027	0.0057 ± 0.0025	0.0055 ± 0.0020
NIRv	0.0056 ± 0.0012	0.0029 ± 0.0009	0.0027 ± 0.0007

**Table A4**

Parameter settings used in the Cubist regression model.

Parameter	Value
n_rules	500
n_committees	5
neighbors	3
Other parameters	Default values

**Table A5**

Proportion of greening and browning trend pixels in each processing levels of NDVI and NIRv for three different periods. Values in parenthesis indicate the proportion of statistically significant trend pixels.

		1982–1999		2000–2021		1982–2021	
Greening		<b>NDVI</b>	<b>NIRv</b>	<b>NDVI</b>	<b>NIRv</b>	<b>NDVI</b>	<b>NIRv</b>
	LTDR	85.23% (35.49%)	88.67% (37.36%)	56.27% (20.36%)	44.69% (13.69%)	82.46% (61.35%)	77.33% (51.97%)
	Cross-calibrated	77.57% (29.49%)	76.70% (28.31%)	60.08% (22.66%)	52.60% (18.10%)	92.71% (77.06%)	89.70% (70.17%)
	Orbit-corrected	77.62% (27.37%)	76.91% (24.40%)	63.89% (25.65%)	58.67% (24.00%)	89.97% (74.87%)	87.74% (70.15%)
	Harmonized	71.31% (19.58%)	75.82% (24.54%)	73.24% (32.10%)	75.62% (35.64%)	86.55% (66.71%)	86.53% (70.37%)
Browning		<b>NDVI</b>	<b>NIRv</b>	<b>NDVI</b>	<b>NIRv</b>	<b>NDVI</b>	<b>NIRv</b>
	LTDR	14.77% (1.02%)	11.33% (1.00%)	43.73% (12.95%)	55.31% (20.65%)	17.54% (5.39%)	22.67% (7.12%)
	Cross-calibrated	22.43% (1.94%)	23.30% (2.28%)	39.92% (10.59%)	47.40% (15.31%)	7.29% (1.70%)	10.30% (2.57%)
	Orbit-corrected	22.38% (2.06%)	23.09% (2.40%)	36.11% (10.10%)	41.33% (13.57%)	10.03% (3.73%)	12.26% (4.43%)
	Harmonized	28.69% (2.39%)	24.18% (1.91%)	26.76% (5.28%)	24.38% (3.98%)	13.45% (4.37%)	13.47% (5.57%)

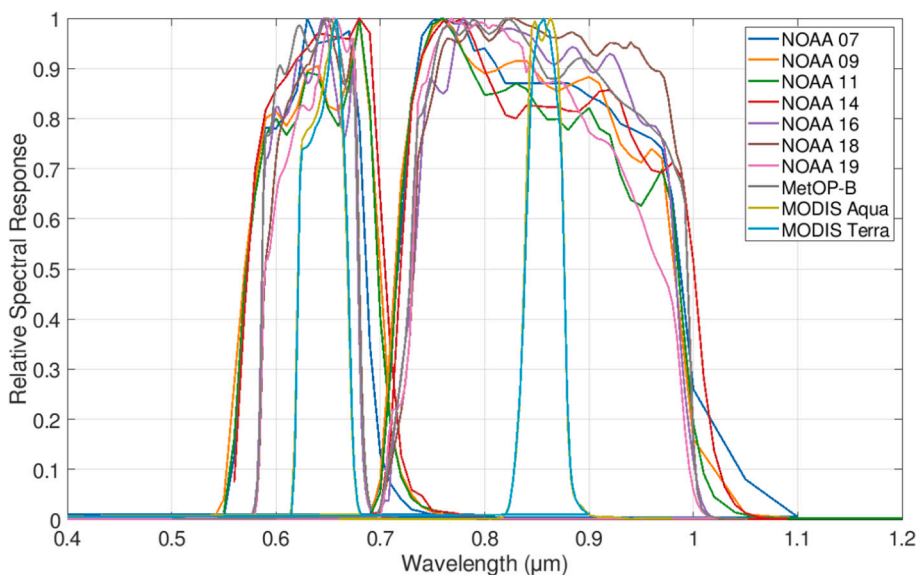


Fig. A1. Relative spectral response from AVHRR satellites and MODIS obtained from <https://cloudsway2.larc.nasa.gov>.

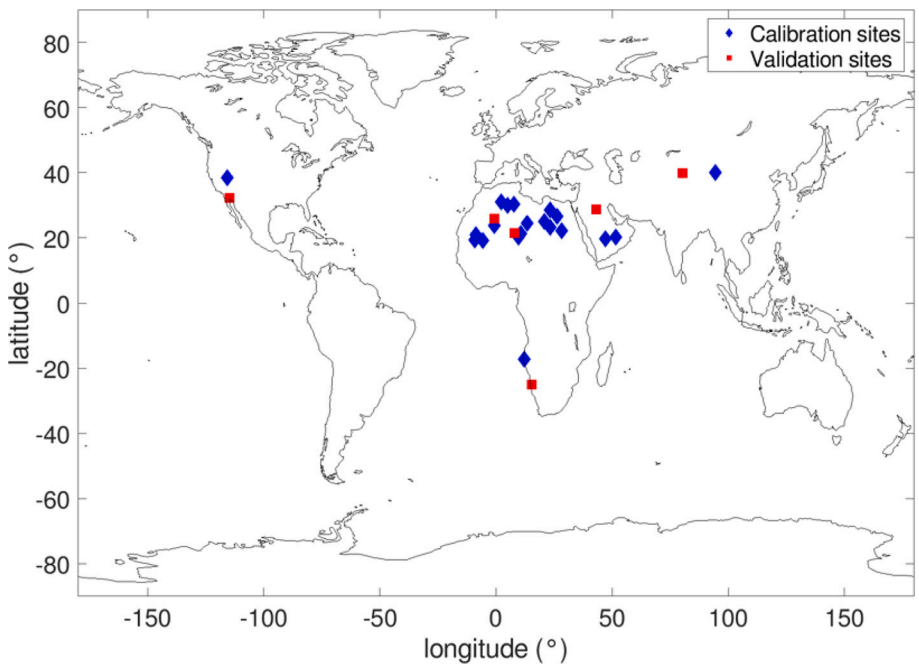


Fig. A2. Global distribution of Pseudo-invariant Calibration Site (PICS) used for calibration and validation of AVHRR time series. Total 26 PICS were used for calibration (20 sites) and validation (6 sites). Blue diamond indicates calibration sites, and red square indicate validation sites. (For interpretation of the references to colour in this figure legend, the reader is referred to the web version of this article.)



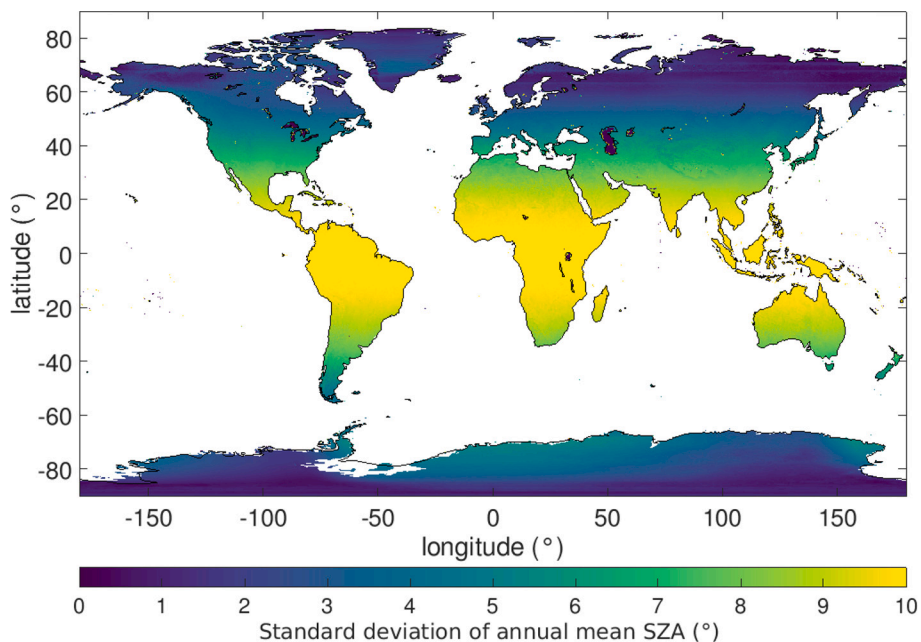


Fig. A3. Standard deviation of annual mean solar zenith angle at overpass time in each pixel from 1982 to 2021.

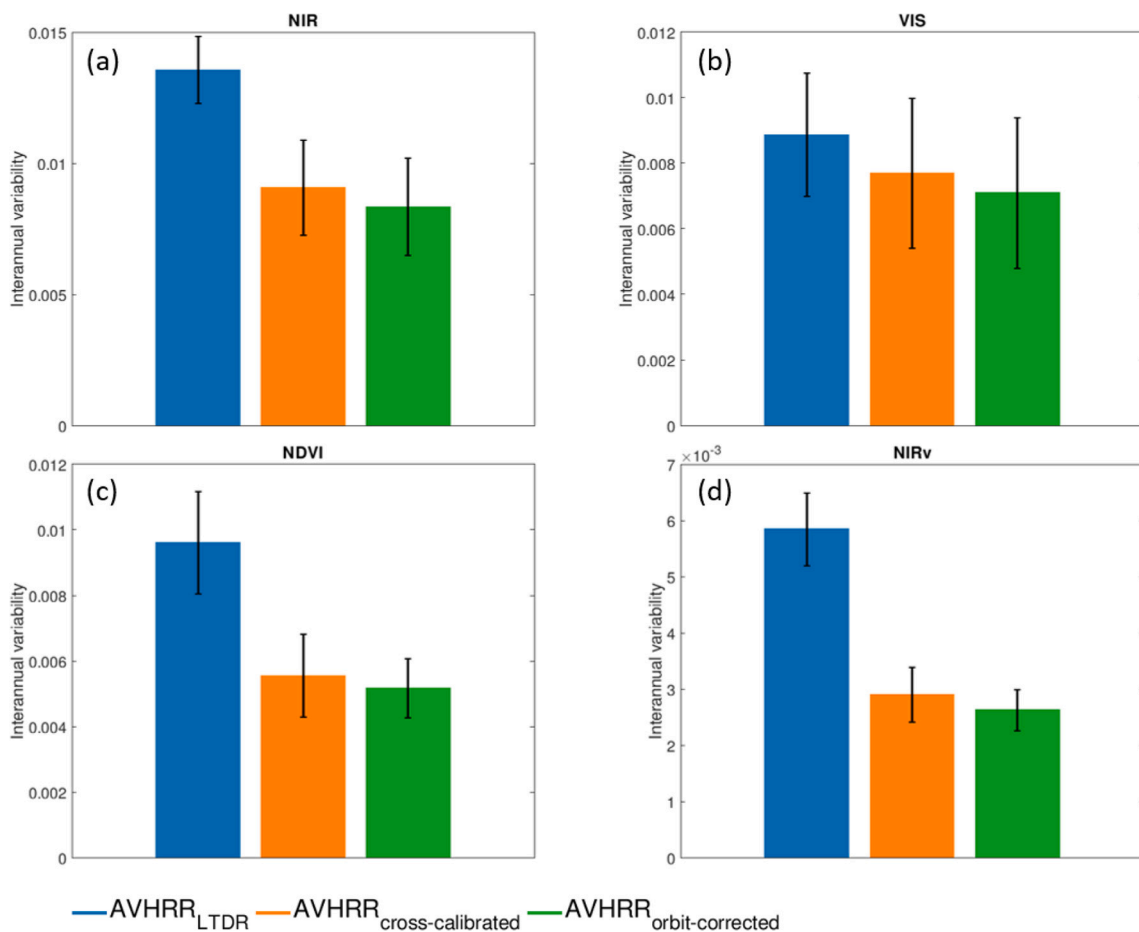


Fig. A4. Interannual variability of NIR, Red reflectance, NDVI, and NIRv for 1982–2021 at 26 Pseudo-invariant Calibration Site (PICS). The different colors represent LTDR (blue), cross-calibrated (orange), and orbit-corrected (green) respectively. Black error bars indicate the standard deviation of each interannual variability in each processing level of data. (For interpretation of the references to colour in this figure legend, the reader is referred to the web version of this article.)

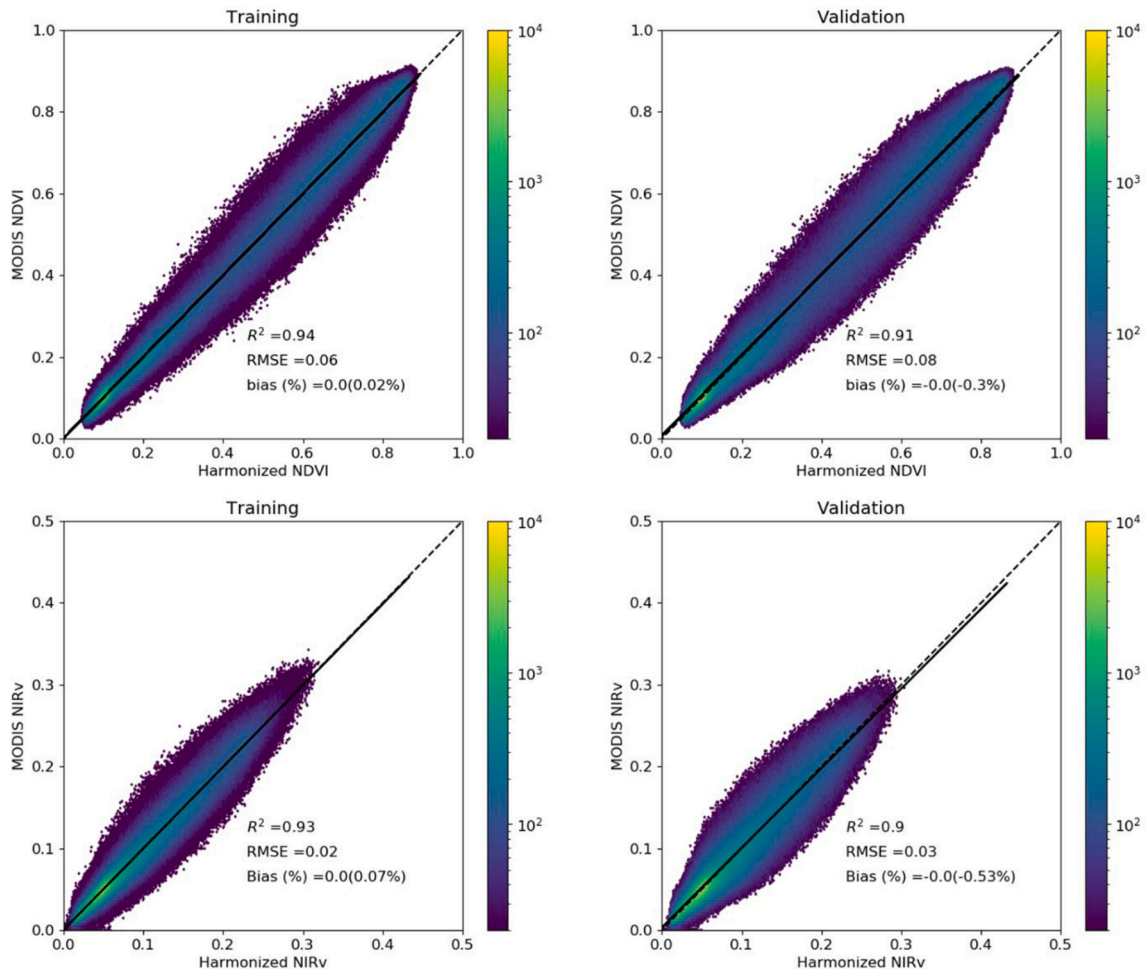
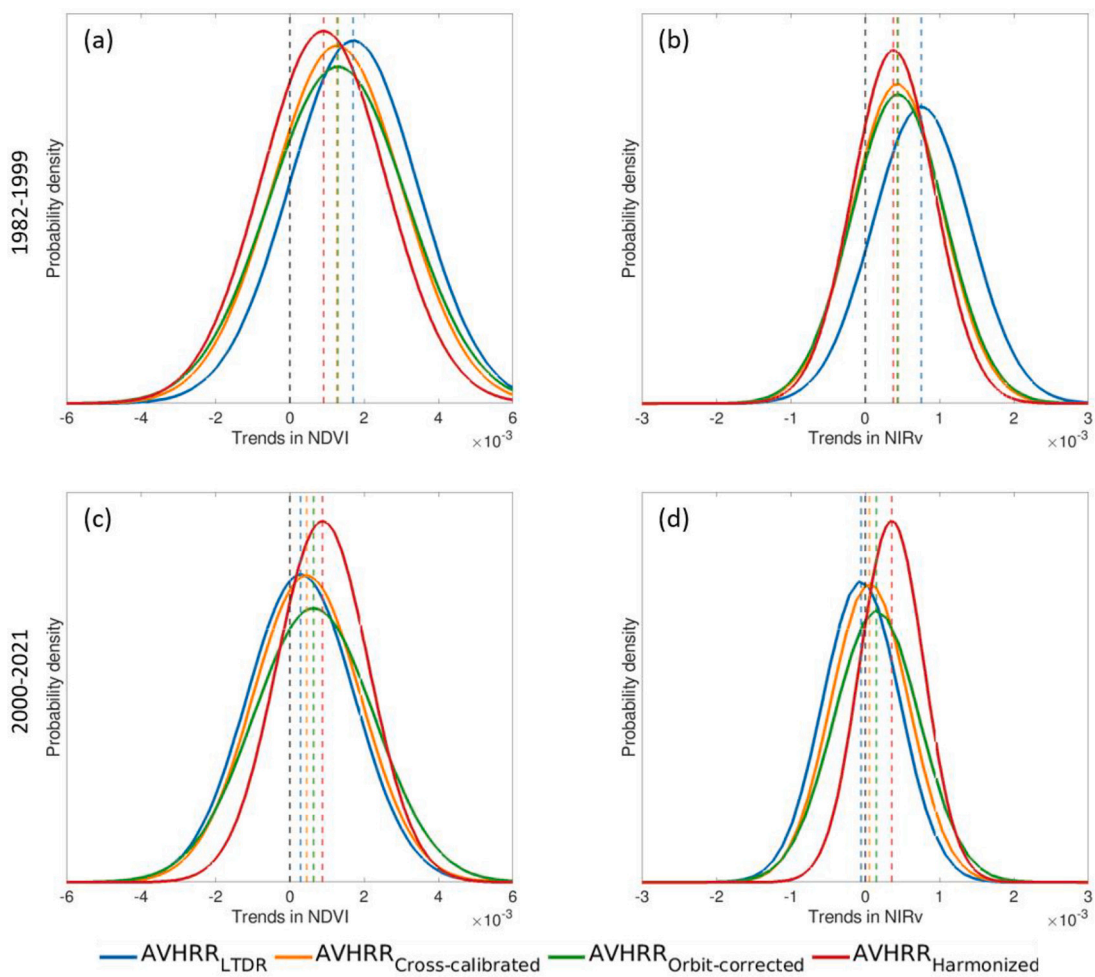


Fig. A5. The performance of the Cubist model for NDVI and NIRv in training and validation.



**Fig. A6.** Probability density function of long-term trends in different processing levels of AVHRR NDVI (a,c), and NIRv (b,d). The different colors represent original LTDR (blue), cross-calibrated (orange), orbit-corrected (green), and harmonized (red) NDVI and NIRv, respectively. The colored vertical lines indicate the averaged trends in each data. (For interpretation of the references to colour in this figure legend, the reader is referred to the web version of this article.)

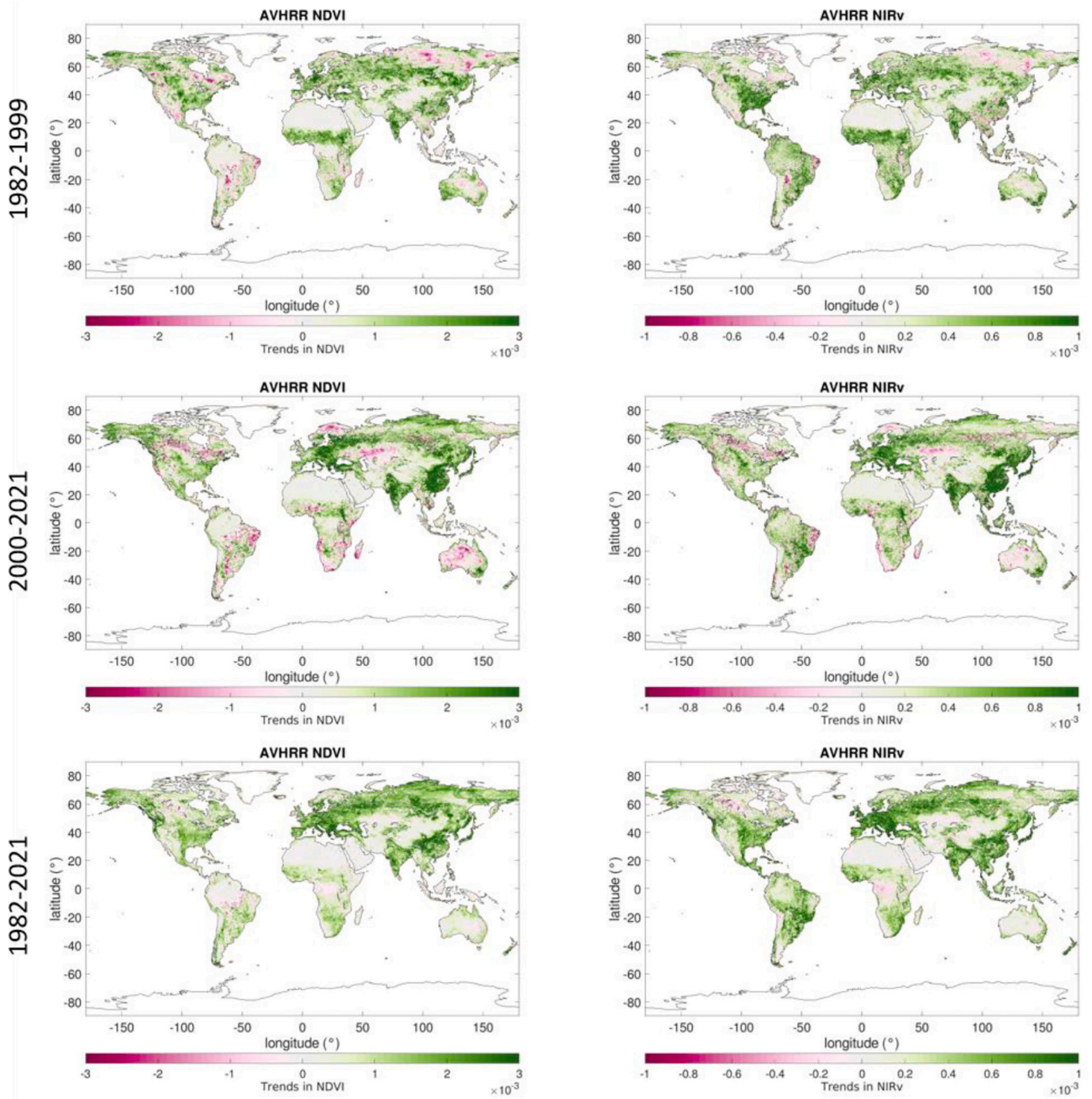
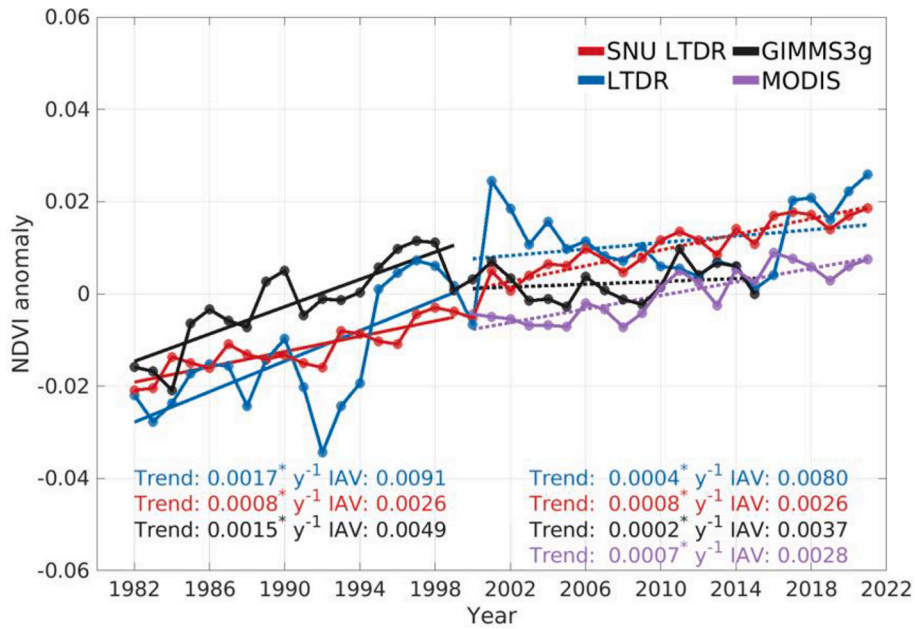
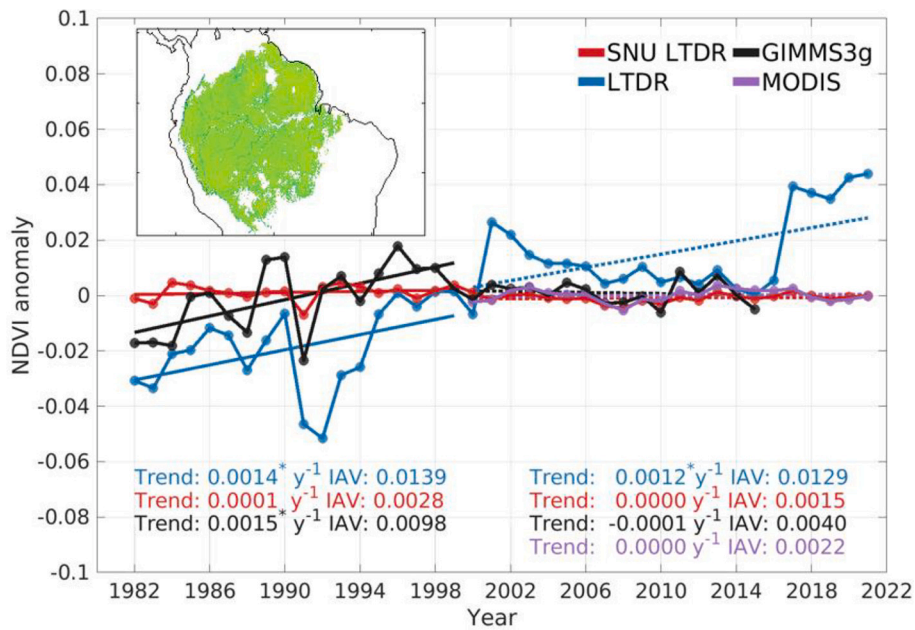


Fig. A7. Spatial patterns of trends in AVHRR<sub>harmonized</sub> NDVI and NIRv. Statistically significant trends (Mann-Kendall test,  $p < 0.1$ ) are colour-coded. Grey areas show vegetated land with statistically insignificant trends.



**Fig. A8.** Annual growing season anomaly of four NDVI datasets (AVHRR<sub>LTDR</sub>, AVHRR<sub>harmonized</sub>, GIMMS3g, and MODIS). Slope and interannual variability were calculated in different periods (Upper left: 1982–1999; Below right: 2000–2021; GIMMS3g: 2000–2015). The different colors represent AVHRR<sub>LTDR</sub> (LTDR) (blue), AVHRR<sub>harmonized</sub> (SNU LTDR) (orange), GIMMS3g (green), and MODIS (purple) NDVI, respectively. (For interpretation of the references to colour in this figure legend, the reader is referred to the web version of this article.)



**Fig. A9.** Annual growing season anomaly of four NDVI datasets in Amazon evergreen broadleaf forests (AVHRR<sub>LTDR</sub>, AVHRR<sub>harmonized</sub>, GIMMS3g, and MODIS). Slope and interannual variability were calculated in different periods (Upper left: 1982–1999; Below right: 2000–2021; GIMMS3g: 2000–2015). The different colors represent AVHRR<sub>LTDR</sub> (LTDR) (blue), AVHRR<sub>harmonized</sub> (SNU LTDR) (orange), GIMMS3g (green), and MODIS (purple) NDVI, respectively. (For interpretation of the references to colour in this figure legend, the reader is referred to the web version of this article.)

**Appendix B. Supplementary data**

Supplementary data to this article can be found online at <https://doi.org/10.1016/j.rse.2024.114282>.

**References**

Abouali, M., 2023. MATLAB Implementation of Harmonic Analysis of Time Series (HANTS). MATLAB Central File Exchange.

Bacour, C., Briottet, X., Bréon, F.M., Viallefont-Robinet, F., Bouvet, M., 2019. Revisiting Pseudo invariant calibration sites (PICS) over sand deserts for vicarious calibration of optical imagers at 20 km and 100 km scales. *Remote Sens.* 11 (10), 1166.  
 Badgley, G., Field, C.B., Berry, J.A., 2017. Canopy near-infrared reflectance and terrestrial photosynthesis. *Sci. Adv.* 3 (3), e1602244.

- Badgley, G., Anderegg, L.D., Berry, J.A., Field, C.B., 2019. Terrestrial gross primary production: using NIRV to scale from site to globe. *Glob. Chang. Biol.* 25 (11), 3731–3740.
- Beck, H.E., McVicar, T.R., van Dijk, A.I., Schellekens, J., de Jeu, R.A., Bruijnzeel, L.A., 2011. Global evaluation of four AVHRR-NDVI data sets: Intercomparison and assessment against Landsat imagery. *Remote Sens. Environ.* 115 (10), 2547–2563.
- Berner, L.T., Massey, R., Jantz, P., Forbes, B.C., Macias-Fauria, M., Myers-Smith, I., Goetz, S.J., 2020. Summer warming explains widespread but not uniform greening in the Arctic tundra biome. *Nat. Commun.* 11 (1), 4621.
- Bhatt, R., Doelling, D.R., Scarino, B.R., Gopalan, A., Haney, C.O., Minnis, P., Bedka, K.M., 2016. A consistent AVHRR visible calibration record based on multiple methods applicable for the NOAA degrading orbits. Part I: methodology. *J. Atmos. Ocean. Technol.* 33 (11), 2499–2515.
- Brown, M.E., Pinzón, J.E., Didan, K., Morissette, J.T., Tucker, C.J., 2006. Evaluation of the consistency of long-term NDVI time series derived from AVHRR, SPOT-vegetation, SeaWiFS, MODIS, and Landsat ETM+ sensors. *IEEE Trans. Geosci. Remote Sens.* 44 (7), 1787–1793.
- Chen, C., Park, T., Wang, X., Piao, S., Xu, B., Chaturvedi, R.K., Myneni, R.B., 2019. China and India lead in greening of the world through land-use management. *Nat. Sustain.* 2 (2), 122–129.
- Dechant, B., Ryu, Y., Badgley, G., Zeng, Y., Berry, J.A., Zhang, Y., Moya, I., 2020. Canopy structure explains the relationship between photosynthesis and sun-induced chlorophyll fluorescence in crops. *Remote Sens. Environ.* 241, 111733.
- Deering, D.W., Eck, T.F., Banerjee, B., 1999. Characterization of the reflectance anisotropy of three boreal forest canopies in spring–summer. *Remote Sens. Environ.* 67 (2), 205–229.
- Defourny, P., Kirches, G., Brockmann, C., Boettcher, M., Peters, M., Bontemps, S., Santoro, M., 2012. Land cover CCL. In: Product User Guide Version, 2, p. 325.
- Fan, X., Liu, Y., 2016. A global study of NDVI difference among moderate-resolution satellite sensors. *ISPRS J. Photogramm. Remote Sens.* 121, 177–191.
- Fang, J., Lian, X., Ryu, Y., Jeong, S., Jiang, C., Gentine, P., 2023. Reconstruction of a Long-Term Spatially Contiguous Solar-Induced Fluorescence (LCSIF) over 1982–2022 arXiv preprint arXiv:2311.14987.
- Fensholt, R., Rasmussen, K., Nielsen, T.T., Mbwo, C., 2009. Evaluation of earth observation based long term vegetation trends—Intercomparing NDVI time series trend analysis consistency of Sahel from AVHRR GIMMS, Terra MODIS and SPOT VGT data. *Remote Sens. Environ.* 113 (9), 1886–1898.
- Franch, B., Vermote, E.F., Roger, J.C., Murphy, E., Becker-Reshef, I., Justice, C., Devadiga, S., 2017. A 30+ year AVHRR land surface reflectance climate data record and its application to wheat yield monitoring. *Remote Sens.* 9 (3), 296.
- Frankenberg, C., Yin, Y., Byrne, B., He, L., Gentine, P., 2021. Comment on “recent global decline of CO<sub>2</sub> fertilization effects on vegetation photosynthesis”. *Science* 373 (6562), eabg2947.
- Friedl, M., Sulla-Menashe, D., 2022. MODIS/Terra+Aqua Land Cover Type Yearly L3 Global 0.05Deg CMG V061 [Data set]. NASA EOSDIS Land Processes Distributed Active Archive Center. Accessed 2024-02-21 from: <https://doi.org/10.5067/MODIS/MCD12C1.061>.
- Giglio, L., Roy, D.P., 2020. On the outstanding need for a long-term, multi-decadal, validated and quality assessed record of global burned area: caution in the use of advanced very high resolution radiometer data. *Sci. Rem. Sens.* 2, 100007.
- Giglio, L., Roy, D.P., 2022. Assessment of satellite orbit-drift artifacts in the long-term AVHRR FireCILT11 global burned area data set. *Sci. Rem. Sens.* 5, 100044.
- Gitelson, A.A., Kaufman, Y.J., 1998. MODIS NDVI optimization to fit the AVHRR data series—spectral considerations. *Remote Sens. Environ.* 66 (3), 343–350.
- Gutman, G.G., 1999. On the use of long-term global data of land reflectances and vegetation indices derived from the advanced very high resolution radiometer. *J. Geophys. Res. Atmos.* 104 (D6), 6241–6255.
- Hersbach, H., Bell, B., Berrisford, P., Hirahara, S., Horányi, A., Muñoz-Sabater, J., Thépaut, J.N., 2020. The ERA5 global reanalysis. *Q. J. R. Meteorol. Soc.* 146 (730), 1999–2049.
- Hussain, M., Mahmud, I., 2019. pyMannKendall: a python package for non parametric Mann Kendall family of trend tests. *J. Open Sour. Softw.* 4 (39), 1556.
- Jeong, S., Ryu, Y., Dechant, B., Li, X., Kong, J., Choi, W., Chun, J., 2023. Tracking diurnal to seasonal variations of gross primary productivity using a geostationary satellite, GK-2A advanced meteorological imager. *Remote Sens. Environ.* 284, 113365.
- Ju, J., Masek, J.G., 2016. The vegetation greenness trend in Canada and US Alaska from 1984–2012 Landsat data. *Remote Sens. Environ.* 176, 1–16.
- Keenan, T.F., Prentice, I.C., Canadell, J.G., Williams, C.A., Wang, H., Raupach, M., Collatz, G.J., 2016. Recent pause in the growth rate of atmospheric CO<sub>2</sub> due to enhanced terrestrial carbon uptake. *Nat. Commun.* 7 (1), 13428.
- Kolby Smith, W., Reed, S.C., Cleveland, C.C., Ballantyne, A.P., Anderegg, W.R., Wieder, W.R., Running, S.W., 2016. Large divergence of satellite and earth system model estimates of global terrestrial CO<sub>2</sub> fertilization. *Nat. Clim. Chang.* 6 (3), 306–310.
- Latifovic, R., Pouliot, D., Dillabaugh, C., 2012. Identification and correction of systematic error in NOAA AVHRR long-term satellite data record. *Remote Sens. Environ.* 127, 84–97.
- Li, X., Xiao, J., 2019. A global, 0.05-degree product of solar-induced chlorophyll fluorescence derived from OCO-2, MODIS, and reanalysis data. *Remote Sens.* 11 (5), 517.
- Li, C., Xue, Y., Liu, Q., Guang, J., He, X., Zhang, J., Liu, X., 2014. Post calibration of channels 1 and 2 of long-term AVHRR data record based on SeaWiFS data and pseudo-invariant targets. *Remote Sens. Environ.* 150, 104–119.
- Li, M., Cao, S., Zhu, Z., Wang, Z., Myneni, R.B., Piao, S., 2023. Spatiotemporally consistent global dataset of the GIMMS normalized difference vegetation index (PKU GIMMS NDVI) from 1982 to 2022. *Earth Syst. Sci. Data* 15 (9), 4181–4203.
- Liu, Y., Liu, R., Chen, J.M., 2012. Retrospective retrieval of long-term consistent global leaf area index (1981–2011) from combined AVHRR and MODIS data. *J. Geophys. Res. Biogeosci.* 117 (G4).
- Los, S.O., 1998. Estimation of the ratio of sensor degradation between NOAA AVHRR channels 1 and 2 from monthly NDVI composites. *IEEE Trans. Geosci. Remote Sens.* 36 (1), 206–213.
- Los, S.O., North, P.R.J., Grey, W.M.F., Barnsley, M.J., 2005. A method to convert AVHRR normalized difference vegetation index time series to a standard viewing and illumination geometry. *Remote Sens. Environ.* 99 (4), 400–411.
- Mao, D., Wang, Z., Luo, L., Ren, C., 2012. Integrating AVHRR and MODIS data to monitor NDVI changes and their relationships with climatic parameters in Northeast China. *Int. J. Appl. Earth Obs. Geoinf.* 18, 528–536.
- Miura, T., Smith, C.Z., Yoshioka, H., 2021. Validation and analysis of Terra and Aqua MODIS, and SNPP VIIRS vegetation indices under zero vegetation conditions: a case study using Railroad Valley playa. *Remote Sens. Environ.* 257, 112344.
- Myneni, R.B., Ramakrishna, R., Nemani, R., Running, S.W., 1997. Estimation of global leaf area index and absorbed PAR using radiative transfer models. *IEEE Trans. Geosci. Remote Sens.* 35 (6), 1380–1393.
- Nagol, J.R., Vermote, E.F., Prince, S.D., 2014. Quantification of impact of orbital drift on inter-annual trends in AVHRR NDVI data. *Remote Sens.* 6 (7), 6680–6687.
- Pedely, J., Devadiga, S., Masuoka, E., Brown, M., Pinzon, J., Tucker, C., Pinheiro, A., 2007. July. Generating a long-term land data record from the AVHRR and MODIS instruments. In: In 2007 IEEE International Geoscience and Remote Sensing Symposium. IEEE, pp. 1021–1025.
- Piao, S., Wang, X., Park, T., Chen, C., Lian, X.U., He, Y., Myneni, R.B., 2020. Characteristics, drivers and feedbacks of global greening. *Nat. Rev. Earth Environ.* 1 (1), 14–27.
- Pickens, A.H., Hansen, M.C., Hancher, M., Stehman, S.V., Tyukavina, A., Potapov, P., Sherani, Z., 2020. Mapping and sampling to characterize global inland water dynamics from 1999 to 2018 with full Landsat time-series. *Remote Sens. Environ.* 243, 111792.
- Pinzon, J.E., Tucker, C.J., 2014. A non-stationary 1981–2012 AVHRR NDVI3g time series. *Remote Sens.* 6 (8), 6929–6960.
- Prentice, I.C., Harrison, S.P., Bartlein, P.J., 2011. Global vegetation and terrestrial carbon cycle changes after the last ice age. *New Phytol.* 189 (4), 988–998.
- Quinlan, J.R., 1992, November. Learning with continuous classes. In: 5th Australian Joint Conference on Artificial Intelligence, 92, pp. 343–348.
- Randles, C.A., Da Silva, A.M., Buchard, V., Colarco, P.R., Darmenov, A., Govindaraju, R., Flynn, C.J., 2017. The MERRA-2 aerosol reanalysis, 1980 onward. Part I: System description and data assimilation evaluation. *J. Clim.* 30 (17), 6823–6850.
- Roujean, J.L., Leroy, M., Deschamps, P.Y., 1992. A bidirectional reflectance model of the Earth's surface for the correction of remote sensing data. *J. Geophys. Res. Atmos.* 97 (D18), 20455–20468.
- Roy, D.P., Li, Z., Zhang, H.K., Huang, H., 2020. A continuous United States analysis of the impact of Landsat 5 orbit drift on the temporal consistency of Landsat 5 thematic mapper data. *Remote Sens. Environ.* 240, 11701.
- Santamaria-Artigas, A., Vermote, E.F., Franch, B., Roger, J.C., Skakun, S., 2021. Evaluation of the AVHRR surface reflectance long term data record between 1984 and 2011. *Int. J. Appl. Earth Obs. Geoinf.* 98, 102317.
- Schaaf, C.B., Gao, F., Strahler, A.H., Lucht, W., Li, X., Tsang, T., Roy, D., 2002. First operational BRDF, albedo nadir reflectance products from MODIS. *Remote Sens. Environ.* 83 (1–2), 135–148.
- Tian, F., Fensholt, R., Verbesselt, J., Grogan, K., Horion, S., Wang, Y., 2015. Evaluating temporal consistency of long-term global NDVI datasets for trend analysis. *Remote Sens. Environ.* 163, 326–340.
- Trishchenko, A.P., Cihlar, J., Li, Z., 2002. Effects of spectral response function on surface reflectance and NDVI measured with moderate resolution satellite sensors. *Remote Sens. Environ.* 81 (1), 1–18.
- Tucker, C.J., 1979. Red and photographic infrared linear combinations for monitoring vegetation. *Remote Sens. Environ.* 8 (2), 127–150.
- Tucker, C.J., Pinzon, J.E., Brown, M.E., Slayback, D.A., Pak, E.W., Mahoney, R., El Saleou, N., 2005. An extended AVHRR 8-km NDVI dataset compatible with MODIS and SPOT vegetation NDVI data. *Int. J. Remote Sens.* 26 (20), 4485–4498.
- Van Leeuwen, W.J., Orr, B.J., Marsh, S.E., Herrmann, S.M., 2006. Multi-sensor NDVI data continuity: uncertainties and implications for vegetation monitoring applications. *Remote Sens. Environ.* 100 (1), 67–81.
- Vermote, E., 2021. LTDR AVHRR Products (Version 5) User's Guide.
- Vermote, E., Justice, C.O., Bréon, F.M., 2008. Towards a generalized approach for correction of the BRDF effect in MODIS directional reflectances. *IEEE Trans. Geosci. Remote Sens.* 47 (3), 898–908.
- Wang, Z., Schaaf, C.B., Sun, Q., Shuai, Y., Román, M.O., 2018. Capturing rapid land surface dynamics with collection Y006 MODIS BRDF/NBAR/albedo (MCD43) products. *Remote Sens. Environ.* 207, 50–64.
- Wang, S., Zhang, Y., Ju, W., Chen, J.M., Ciais, P., Cescaati, A., Peñuelas, J., 2020. Recent global decline of CO<sub>2</sub> fertilization effects on vegetation photosynthesis. *Science* 370 (6522), 1295–1300.
- Wang, S., Zhang, Y., Ju, W., Qiu, B., Zhang, Z., 2021. Tracking the seasonal and inter-annual variations of global gross primary production during last four decades using satellite near-infrared reflectance data. *Sci. Total Environ.* 755, 142569.
- Wang, Z., Wang, H., Wang, T., Wang, L., Liu, X., Zheng, K., Huang, X., 2022. Large discrepancies of global greening: indication of multi-source remote sensing data. *Glob. Ecol. Conserv.* 34, e02016.
- Wanner, W., Li, X., Strahler, A.H., 1995. On the derivation of kernels for kernel-driven models of bidirectional reflectance. *J. Geophys. Res. Atmos.* 100 (D10), 21077–21089.

- Xiao, Z., Liang, S., Wang, J., Xiang, Y., Zhao, X., Song, J., 2016. Long-time-series global land surface satellite leaf area index product derived from MODIS and AVHRR surface reflectance. *IEEE Trans. Geosci. Remote Sens.* 54 (9), 5301–5318.
- Zeng, Y., Hao, D., Huete, A., Dechant, B., Berry, J., Chen, J.M., Chen, M., 2022. Optical vegetation indices for monitoring terrestrial ecosystems globally. *Nat. Rev. Earth Environ.* 3 (7), 477–493.
- Zhang, Y., Song, C., Band, L.E., Sun, G., Li, J., 2017. Reanalysis of global terrestrial vegetation trends from MODIS products: Browning or greening? *Remote Sens. Environ.* 191, 145–155.
- Zhu, Z., Bi, J., Pan, Y., Ganguly, S., Anav, A., Xu, L., Myneni, R.B., 2013. Global data sets of vegetation leaf area index (LAI) 3g and fraction of photosynthetically active radiation (FPAR) 3g derived from global inventory modeling and mapping studies (GIMMS) normalized difference vegetation index (NDVI3g) for the period 1981 to 2011. *Remote Sens.* 5 (2), 927–948.
- Zhu, Z., Piao, S., Myneni, R.B., Huang, M., Zeng, Z., Canadell, J.G., Zeng, N., 2016. Greening of the earth and its drivers. *Nat. Clim. Chang.* 6 (8), 791–795.
- Zhu, Z., Zeng, H., Myneni, R.B., Chen, C., Zhao, Q., Zha, J., MacLachlan, I., 2021. Comment on “recent global decline of CO<sub>2</sub> fertilization effects on vegetation photosynthesis”. *Science* 373 (6562) eabg5673.